J. Fluid Mech., page 1 of 31
doi:10.1017/S0022112010004039

Wave scattering by ice floes and polynyas of arbitrary shape

L. G. BENNETTS[1]† AND T. D. WILLIAMS[2]

[1]Department of Mathematics and Statistics, University of Otago, P.O. Box 56, Dunedin 9054, New Zealand

[2]Department of Mathematics, University of Bristol, University Walk, Bristol BS8 1TW, UK

(Received 8 April 2010; revised 27 July 2010; accepted 27 July 2010)

An efficient solution method is presented for linear and time-harmonic water-wave scattering by two classes of a three-dimensional hydroelastic system. In both cases, the fluid domain is of infinite horizontal extent and finite depth. The fluid surface is either open, except in a finite region where it is covered by a thin-elastic plate, which represents an ice floe, or fully covered by a plate, except in a finite region where it is open, which represents an ice polynya. The approach outlined herein permits the boundary between the ice-covered and free-surface fluid regions to be described by an arbitrary smooth curve. To solve the governing equations of the full three-dimensional linear problem, they are first projected onto the horizontal plane by using an approximation theory that combines an expansion of the vertical motion of the fluid in a finite set of judiciously chosen modes with a variational principle. This generates a system of two-dimensional partial differential equations that are converted into a set of one-dimensional integro-differential equations using matrices of Green's functions, which are solved numerically through an application of the Galerkin technique. A numerical results section justifies the consideration of an arbitrarily shaped boundary by comparing the response of differently shaped floes and polynyas over a range of relevant wavenumbers. Comparisons are made in terms of the magnitude and direction of the far-field scattering response, and also the maximum average curvature of the floe and the maximum wave elevation within the polynya.

Key words: sea ice, wave scattering

1. Introduction

Sea ice circumscribes both poles, forming a natural barrier from ocean wave energy impacting on the inner masses of ice, such as the ice shelves and tongues that characterise the coasts of Antarctica and Greenland. Its fate, in the advent of global warming, is of fundamental importance to both the global climate and engineers working on offshore operations in the polar regions.

Ocean waves are partially reflected and partially transmitted at the interface between the open ocean and the ice pack, with the surviving proportion of the wave then gradually attenuating as it penetrates deeper into the ice-covered ocean. This is due to scattering and other processes, namely inelastic bending of the ice, hydrodynamical

† Email address for correspondence: lbennetts@maths.otago.ac.nz

turbulence and wave-induced collisions. In particular, sea ice is responsible for filtering out high-frequency waves at an early stage; whereas long swell waves may reach tens to hundreds of kilometres into the ice-covered ocean (Squire *et al.* 1995; Squire 2007).

The structure of a region of sea ice will depend on a number of factors and predominantly its proximity to the open ocean. When a wave enters the ice-covered ocean it induces a flexural response in the ice, and this imposes a strain that can fracture the ice into smaller ice floes if the amplitude is sufficient (Langhorne, Squire & Haskell 2001). For this reason, the outskirts of the ice pack are a combination of relatively small floes and ice cakes, separated by open water. When wave activity is present, this is a highly dynamic area and is responsible for the aforementioned filtering of high-frequency waves.

Beyond this zone, where the strength of the travelling waves has been reduced sufficiently that it will no longer cause breakup, the ice covering is far more continuous but is proliferated by imperfections such as cracks, ridges and polynyas. The latter are pools or lakes in the ice cover that are formed either through offshore winds separating the ice pack (latent heat polynyas) or by a localised upwelling of warm water (sensible heat polynyas) or by a combination of both.

Recently, a number of models of wave evolution through ice-covered waters on meaningful scales have been published in both two-dimensional (Kohout & Meylan 2008; Squire, Vaughan & Bennetts 2009; Vaughan, Bennetts & Squire 2009; Williams & Squire 2010) and three-dimensional (Bennetts & Squire 2009; Peter & Meylan 2009; Bennetts *et al.* 2010) contexts. Whilst two-dimensional models have much merit and the simplicity they offer is convenient for analytical and numerical analysis, it is recognised that scattering also diffracts wave energy laterally and an accurate representation demands a fully three-dimensional examination.

At the heart of both the large-scale two-dimensional and three-dimensional models are solutions for individual scatterers, such as ice floes and polynyas. Particularly for the more computationally demanding three-dimensional description, at this level it is necessary to balance the desire to accurately model the local effects, by not overly stylising the geometry, with the numerical expense of a fully heterogeneous description. To this end, the current work outlines a method that allows the efficient solution of a floe or a polynya of arbitrary shape.

The last two decades have seen a surge of research in the area of hydroelastic scattering with applications to sea ice. Therein, the regular assumptions of linear wave theory are common, as is the identification of sea ice as a thin-elastic plate and the imposition of time-harmonic conditions. We retain these foundations. Matters have progressed to the point at which isolated features in two dimensions, such as thickness variations (Williams & Squire 2004; Bennetts, Biggs & Porter 2007), cracks (Squire & Dixon 2000; Evans & Porter 2003) and separations (or leads) (Chung & Linton 2005) in the ice cover, can be accommodated. A physically correct draught can also be incorporated (Bennetts *et al.* 2007; Williams & Porter 2009), an effect that can have marked effects on multiple scattering results (Williams & Squire 2010).

Three-dimensional models of wave–floe interactions have also been developed, although many of these are restricted to circular geometry. For example, Meylan & Squire (1996) and Peter, Meylan & Chung (2004) solve for a circular floe of constant thickness and zero draught, whilst Bennetts, Biggs & Porter (2009) allow for axisymmetric variations and partial submergence. A coupled boundary element and finite element method for obtaining the scattering response of a floe of constant thickness and zero draught but of arbitrary shape is outlined in Meylan (2002) and

Wang & Meylan (2004), which requires the numerical discretisation of the floe to acquire its *in-vacuo* dry modes. Such an approach, however, would not lend itself readily to the polynya problem, in which the ice cover is of infinite extent. From this standpoint the floe and polynya problems are distinguished from one another, whereas in the method that will be outlined in this work they are unified. Sturova (2001) also tackles the problem of a floe of constant thickness and arbitrary shape but on shallow water, by converting the governing equations into a system of boundary integral equations and produces a numerical solution by discretising these.

In the parallel field of wave interaction with pontoon-type very large floating structures (VLFSs), which shares the same fundamental mathematical model, solution methods for three-dimensional elastic plates have also been generated. These are often of a highly numerical nature and concentrate on transient effects, although it is worth highlighting the matched asymptotic expansion method of Ohkusu & Namba (2004) for a finite rectangular plate of zero draught on shallow water. A review of the recent work on pontoon-type VLFSs can be found in Watanabe, Utsunomiya & Wang (2004) and a more recent review, Squire (2008), draws together the two fields of sea ice research and VLFS modelling.

No solutions (to the authors' knowledge) appear to have been generated for three-dimensional diffraction by a polynya or, more generally, by an opening in a floating elastic plate. This is likely to be, in part, a consequence of the difficulty presented by the infinite extent of the ice cover, as discussed above. However, the related solution method for wave scattering by finite straight-line cracks of Porter & Evans (2007) using source functions is of note. This is summarised, along with all of the other works referenced above, in the extensive recent review of Squire (2007).

Waves travel through a region of ice-covered fluid in the form of flexural-gravity waves, which satisfy a high-order condition at the interface of the two media that describes restoring due to the elastic response of the ice in addition to gravity. This is as opposed to pure gravity waves that exist when the fluid is unloaded, and satisfy the regular free-surface condition. Each of these two states possesses its own distinct wavenumber and, as a wave encounters a boundary between them, it excites a scattering response, so that only part of the wave survives with the remainder being radiated across the directional spectrum.

To allow for a boundary of arbitrary shape between the ice-covered and free-surface regions of the fluid domain at a low computational cost, we utilise approximation methods that are capable of reproducing the full-linear solution. The first of these involves an expansion of the vertical motion in the fluid in a finite number of the natural vertical modes of the problem, which are the vertical functions obtained when separation solutions are sought in a region of uniform geometry. This approach is common in solution methods for both two-dimensional (e.g. Fox & Squire 1994; Linton & Chung 2003; Manam, Bhattarchajee & Sahoo 2006) and three-dimensional (e.g. Peter *et al.* 2004) hydroelastic wave-scattering problems, in which the fluid is of finite depth. Such an expansion was also adopted by Bennetts *et al.* (2007), who used it in conjunction with a variational principle, derived from the Hamiltonian of the system, to produce a set of vertically averaged equations – these being the descendants of the extended mild-slope equations that are used for free-surface flows (Porter & Staziker 1995). In the current work, the same combination of vertical modes and variational principle is employed. However, while the motivation of Bennetts *et al.* (2007) was in investigating thickness variations and a non-zero draught in a two-dimensional setting, our principal aim in this work is to reduce geometrical complexity in the horizontal plane to a manageable level.

The use of vertical averaging also allows for the incorporation of a non-zero draught in our three-dimensional model, and the numerical implementation of this improves on that of Bennetts *et al.* (2007). It is well established that a potential flow around a geometrical corner with Neumann–Neumann boundary conditions induces a point singularity in the fluid's velocity field of order $-1/3$, and incorporating this singularity into a solution method will enhance its convergence properties. Williams & Porter (2009) have recently shown that using Gegenbauer polynomials to embed the same singular behaviour at a corner with a thin-elastic plate condition on one of the surfaces (retaining a Neumann condition on the other) results in accelerated convergence in their approximation scheme. A similar phenomenon at the end of a submerged, thin, porous plate (where Robin conditions are applied on both sides of the plate) has also been demonstrated by Evans & Peter (2009). Whilst Bennetts *et al.* (2007) used a direct correspondence of the structure of the fluid velocity beneath the ice edge to that beneath the rest of the ice cover, we aim to capture the velocity at the corner in a small number of modes by incorporating the work of Williams & Porter (2009). Moreover, the modification of the original approximation of Bennetts *et al.* (2007) to allow for an expansion beneath the ice edge of a different dimension to that of the surrounding ice-covered and free-surface fluid regions is essential to the success of this approach.

A new system of governing equations, which exists only in the horizontal plane, remains to be solved. This is converted into a finite set of one-dimensional integro-differential equations, posed on the boundary that divides the ice-covered and free-surface fluid regions, through the use of matrices of Green's functions. In order to obtain an efficient numerical solution of the integro-differential system and assuming the boundary is represented by a smooth simple contour, we invoke the Galerkin technique, with a basis of Fourier modes, to leave a linear system of equations to be solved for a finite set of constant values.

The solution method briefly described above is outlined in §§ 2 and 3 and is prefaced by the governing equations of the full-linear problem. In § 4, a simple representation for the diffracted wave in the far-field is derived and its relationship to energy conservation is defined. A selection of numerical results is presented in § 5 that briefly demonstrates the convergence properties of the method. It then justifies the need to model the shape of a floe or polynya in order to recreate the motions they undergo due to wave forcing and also their scattering response, both in terms of direction and magnitude. To finish, a summary is given and conclusions are made in § 6. An analytical deconstruction of the method when the floe or polynya is circular is given in the Appendix.

2. Preliminaries and vertical expansion

2.1. *The full-linear equations*

In this paper, we examine two classes of geometrical configuration, one where an ice floe floats on a fluid surface, the other in which a polynya (or pool) exists in an otherwise continuous floating ice sheet. Much of the notation used to define these configurations is shared and we will begin in a general setting. Therefore, consider a fluid domain and let the horizontal plane it occupies be defined by the Cartesian coordinates $\boldsymbol{x}=(x, y)$ and suppose that this stretches to infinity in all directions. In the absence of ice cover, the fluid domain is of a constant finite depth h and we set the upward-pointing vertical coordinate z to have its origin coincide with the equilibrium surface of the fluid, so that $z=-h$ denotes the sea bed.

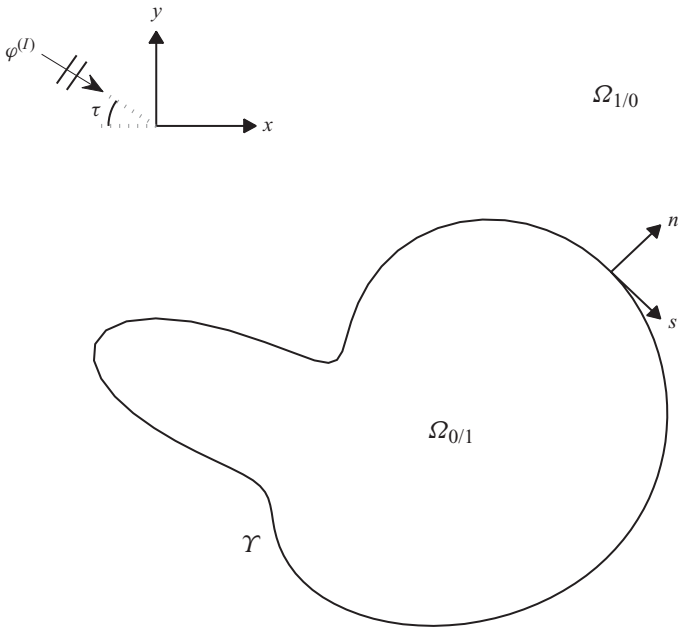

FIGURE 1. Schematic of the geometry in the horizontal plane.

Sea ice, of constant thickness D, covers a portion of the fluid surface, which is left unspecified for the present. In order to ensure neutral buoyancy of the ice we allow for a draught of $d = (\rho_i/\rho_w)D = 0.9D$, where $\rho_i = 922.5\,\mathrm{kg\,m^{-3}}$ and $\rho_w = 1025\,\mathrm{kg\,m^{-3}}$ are the densities of the ice and water, respectively, so that it satisfies the Archimedean principle.

We now partition the horizontal plane into two regions using the closed and simple contour Υ of length 2γ, which is parameterised using the arclength s, such that $s \in (-\gamma, \gamma)$. The area of the horizontal plane occupied by free-surface fluid will be denoted as Ω_0 and that occupied by ice-covered fluid is Ω_1. For the problem of wave scattering by a polynya the region Ω_0 is the finite domain domain enclosed by Υ and Ω_1 is the exterior, whereas in the floe problem these rôles are reversed. To facilitate the solution process we will suppose the contour Υ to be smooth. An example of the geometrical configuration described above is shown in figures 1 and 2.

The system of fluid and ice is set in motion by a plane incident wave that induces a flexural response in the ice. If we consider the problem to be time harmonic, then the position of the underside of the ice may be written as

$$z = -d + \mathrm{Re}(W\mathrm{e}^{-\mathrm{i}\omega t}). \tag{2.1}$$

Here ω is some prescribed angular frequency and $W = W(\boldsymbol{x})$ is an unknown displacement function defining the oscillations of the ice, which must be calculated as part of the solution process.

Under the regular assumptions of linear motions, the properties of the fluid are defined through a velocity potential $\Phi = \Phi(\boldsymbol{x}, z, t)$, so that the velocity field is retrieved from $(\nabla, \partial_z)\Phi$ where $\nabla = (\partial_x, \partial_y)$. Imposing time-harmonic conditions we may write $\Phi(\boldsymbol{x}, z, t) = \mathrm{Re}\{(g/\mathrm{i}\omega)\varphi(\boldsymbol{x}, z)\mathrm{e}^{-\mathrm{i}\omega t}\}$, where $g = 9.81\,\mathrm{m\,s^{-2}}$ is acceleration due to gravity. The (reduced) velocity potential φ satisfies Laplace's equation in the fluid domain

$$\nabla^2\varphi + \partial_z^2\varphi = 0 \quad (\boldsymbol{x} \in \mathbb{R}^2), \tag{2.2}$$

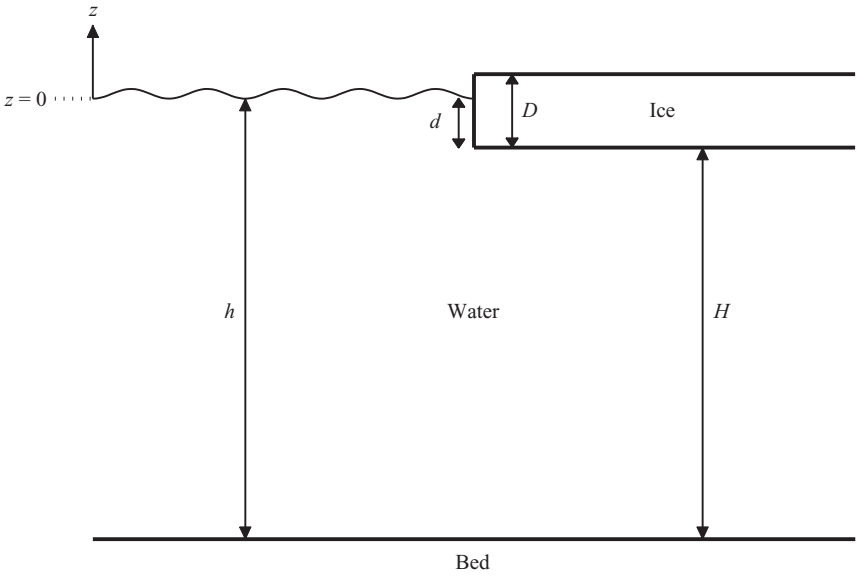

FIGURE 2. Schematic of the geometry in the vertical plane.

for $-h < z < 0$ when $\boldsymbol{x} \in \Omega_0$ and $-h < z < -d$, when $\boldsymbol{x} \in \Omega_1$. It is also subject to the bed condition $\partial_z \varphi = 0$ on $z = -h$.

When the fluid is unloaded and the restoring force is gravity alone, the velocity potential obeys the linearised free-surface condition

$$\partial_z \varphi = \sigma \varphi \quad (z = 0), \tag{2.3}$$

where $\sigma = \omega^2/g$ is a frequency parameter. In comparison, at the linearised fluid–ice interface, $z = -d$, the velocity potential is linked to the displacement function W through the equations

$$(1 - \sigma d)W + \beta \nabla^4 W - \varphi = 0, \quad \partial_z \varphi = \sigma W, \tag{2.4}$$

for $\boldsymbol{x} \in \Omega_1$. In the above equation, β is a scaled version of the flexural rigidity of the ice, which is defined by $\beta = Y D^3/\{12(1-\nu^2)\rho_w g\}$. The further parameters that appear in this definition are Poisson's ratio for sea ice $\nu = 0.3$ and Young's modulus for sea ice $Y = 6 \times 10^9$ Pa.

On the boundary, Υ, that separates the ice-covered and ice-free fluid regions, the displacement function, W, must satisfy the so-called free-edge conditions, which ensure that the ice edge experiences no bending moment and shearing stress. These conditions may be expressed as

$$\beta \nabla^2 W - \tilde{\beta}\left(\partial_s^2 + \Theta' \partial_n\right) W = 0 \tag{2.5a}$$

and

$$\beta \partial_n \nabla^2 W + \tilde{\beta} \partial_s (\partial_s \partial_n - \Theta' \partial_s) W = 0, \tag{2.5b}$$

for $\boldsymbol{x} \in \Upsilon$, where $\tilde{\beta} = (1 - \nu)\beta$. Here $\partial_s = \boldsymbol{s} \cdot \nabla$ and $\partial_n = \boldsymbol{n} \cdot \nabla$, with $\boldsymbol{s}$ a unit vector tangential to Υ, and $\boldsymbol{n}$ a normal vector that points away from Ω_0, with its direction defined as $(\cos\Theta, \sin\Theta)$ $(\Theta = \Theta(s))$ with respect to the horizontal Cartesian frame. We note that the differential operators ∂_n and ∂_s do not in general commute, and

instead the identity

$$\partial_s \partial_n - \Theta' \partial_s \equiv \partial_n \partial_s \tag{2.6}$$

holds (see Porter & Porter 2004). An alternative form of the shearing stress condition (2.5*b*) is therefore possible, but only the one given above is suitable for the solution procedure that will be described in § 3. Furthermore, for each point v at which the boundary Υ is not smooth this quantity is continuous (R. Porter, personal communication 2006; de Veubeke 1979), that is

$$[\partial_n \partial_s W]_{v-} = [\partial_n \partial_s W]_{v+}, \tag{2.7}$$

although the condition will not be required for the present work, as we restrict ourselves to smooth boundaries.

To fully define the mathematical problem, we now need only to specify how diffracted waves radiate away from the floe or polynya. This property differs depending on the problem under consideration and it is pertinent to first define the respective incident waves. For the floe problem, in which the far-field is ice free, we define the incident wave as $\varphi^{(I)} \equiv \phi^{(I)} = \phi^{(I)}(\boldsymbol{x}, z)$, with

$$\phi^{(I)} = \mathrm{e}^{\mathrm{i}k_0(x\cos\tau + y\sin\tau)} \cosh\{k_0(z+h)\}, \tag{2.8}$$

where k_0 is the propagating wavenumber in the free-surface fluid (to be defined shortly) and τ defines the angle at which the incident wave travels with respect to the x-axis (see figure 1). Similarly, when the far-field is ice covered, we denote the incident wave as $\varphi^{(I)} \equiv \psi^{(I)} = \psi^{(I)}(\boldsymbol{x}, z)$, such that

$$\psi^{(I)} = \mathrm{e}^{\mathrm{i}\kappa_0(x\cos\tau + y\sin\tau)} \cosh\{\kappa_0(z+h)\}, \tag{2.9}$$

and κ_0 is the propagating wavenumber in the ice-covered fluid (also to be defined shortly). We note that the velocity potential for the floe and polynya geometries must satisfy the Sommerfeld radiation condition

$$r^{1/2}(\partial_r - \mathrm{i}k_0)\big(\varphi - \phi^{(I)}\big) \to 0 \quad \text{or} \quad r^{1/2}(\partial_r - \mathrm{i}\kappa_0)\big(\varphi - \psi^{(I)}\big) \to 0, \tag{2.10}$$

respectively, as the radial coordinate $r \to \infty$, uniformly in the angular coordinate θ.

2.2. *Expansion of the vertical motion*

The governing equations for either the floe or polynya geometries presented in the previous section present a formidable challenge. As such, our first recourse is to implement an approximation method that reduces the spatial dimension of the problems but that is capable of reproducing the full-linear solution to any desired accuracy. Thus, we let the velocity potential, φ, be expressed as

$$\varphi(\boldsymbol{x}, z) \approx \phi(\boldsymbol{x}, z) = \sum_{n=0}^{N} \phi_n(\boldsymbol{x}) \zeta_n(z) \tag{2.11a}$$

in the free-surface fluid region, and

$$\varphi(\boldsymbol{x}, z) \approx \psi(\boldsymbol{x}, z) = \sum_{n=0}^{N} \psi_n(\boldsymbol{x}) \eta_n(z) \tag{2.11b}$$

in the ice-covered fluid region.

In the above approximations, the z-dependence of the velocity potential has been restricted to a finite dimensional space spanned by the natural vertical modes of the

respective geometries, $\zeta_n(z) = \cosh\{k_n(z+h)\}$ or $\eta_n(z) = \cosh\{\kappa_n(z+h)\}$ $(n = 0, \ldots, N)$. The quantities k_n are the roots k of the free-surface dispersion relation

$$k \tanh(kh) = \sigma, \tag{2.12}$$

with k_0 real and positive and k_n $(n = 1, \ldots, N)$ purely imaginary and ordered such that $0 < -\mathrm{i}k_n < -\mathrm{i}k_{n+1}$. Similarly, the quantities κ_n are the roots κ of the ice-covered (fluid) dispersion relation

$$(1 - \sigma d + \beta\kappa^4)\kappa \tanh(\kappa H) = \sigma, \tag{2.13}$$

where $H = h - d$ denotes the fluid depth beneath the ice. As with the roots of the free-surface dispersion relation, we set κ_0 to be the unique real, positive root and κ_n $(n = 1, \ldots, N)$ to be the roots that lie on the positive imaginary axis and order them in increasing magnitude. The complex roots of the ice-covered dispersion relation can be ignored when creating the approximation (2.11*a*, *b*) due to linear dependence (see Bennetts *et al.* 2007, for details). Instead, the motions that they represent will reappear in an alternative form at a later stage in the solution method. We note here that the set of free-surface fluid modes are orthogonal but that the ice-covered fluid modes are non-orthogonal. Uniform convergence using the latter was established for related two-dimensional problems by Evans & Porter (2003) and Williams (2006, § 4).

By using a sufficiently large value of N, the approximations (2.11*a*, *b*) will improve without limit, so that the full-linear solution may be obtained to any desired level of accuracy. However, we wish to balance this accuracy with the computational expense incurred by increasing the dimension of the approximation. It has been shown previously, for geometries involving partial ice-covering, both in two-dimensional (see Bennetts *et al.* 2007) and simplified three-dimensional (see Bennetts *et al.* 2009) settings, that the above choice of vertical modes produces accurate results for relatively low dimensions.

It remains to define the unknown functions ϕ_n and ψ_n $(n = 0, \ldots, N)$, which exist in the horizontal plane only. A new set of governing equations may be obtained by substituting the approximate forms of the velocity potential given in (2.11*a*, *b*) into a variational principle that is equivalent to the governing equations of the full-linear problem and was presented in Bennetts *et al.* (2007). Combination of this variational principle with the above expansion of the vertical dependence of the solution has the effect of averaging the motion defined by the vertical modes, leaving a finite set of z-independent equations. Despite having no vertical dependence of its own, the method also generates a corresponding approximation of the displacement function $w(\boldsymbol{x}) \approx W(\boldsymbol{x})$ through its association to the velocity potential, which must also be calculated.

In the region of free-surface fluid, we are left to solve the Helmholtz equations

$$\nabla^2 \boldsymbol{\Phi} + \boldsymbol{K}_0^2 \boldsymbol{\Phi} = \boldsymbol{0}, \tag{2.14}$$

for the vector $\boldsymbol{\Phi} = \boldsymbol{\Phi}(\boldsymbol{x}) = (\phi_0(\boldsymbol{x}), \ldots, \phi_N(\boldsymbol{x}))^{\mathrm{T}}$, where the matrix $\boldsymbol{K}_0 = \lceil k_0, \ldots, k_N \rfloor$, and the notation $\lceil \cdot \rfloor$ will be used from this point on to indicate a diagonal matrix. For the domain in which the fluid is ice-covered, the variational principle produces the system of second-order equations

$$\boldsymbol{A}_1 \nabla^2 \boldsymbol{\Psi} + \left(\boldsymbol{A}_1 \boldsymbol{K}_1^2 - \boldsymbol{C}_1 \boldsymbol{o}\boldsymbol{o}^{\mathrm{T}} \boldsymbol{K}_1 \boldsymbol{S}_1\right) \boldsymbol{\Psi} + \sigma \boldsymbol{C}_1 \boldsymbol{o} w = \boldsymbol{0}, \tag{2.15a}$$

which is coupled to the fourth-order equation

$$(1 - \sigma d) w + \nabla^2 \hat{w} - \boldsymbol{o}^{\mathrm{T}} \boldsymbol{C}_1 \boldsymbol{\Psi} = 0. \tag{2.15b}$$

Here $\boldsymbol{o}=(1,\ldots,1)^{\mathrm{T}}$ is a $(N+1)$-length vector and we define the size $(N+1)$-square matrices $\boldsymbol{K}_1=\lceil\kappa_0,\ldots,\kappa_N\rfloor$, $\boldsymbol{C}_1=\lceil\cosh(\kappa_0 H),\ldots,\cosh(\kappa_N H)\rfloor$, $\boldsymbol{S}_1=\lceil\sinh(\kappa_0 H),\ldots,\sinh(\kappa_N H)\rfloor$ and

$$\{\boldsymbol{A}_1\}_{j+1,i+1}=\int_{-h}^{-d}\eta_j\eta_i\,\mathrm{d}z\quad(i,j=0,\ldots,N). \tag{2.16}$$

Equations (2.15*a*, *b*) are to be solved for the vector $\boldsymbol{\Psi}=\boldsymbol{\Psi}(\boldsymbol{x})=(\psi_0(\boldsymbol{x}),\ldots,\psi_N(\boldsymbol{x}))^{\mathrm{T}}$ as well as $w=w(\boldsymbol{x})$ and $\hat{w}=\hat{w}(\boldsymbol{x})$, where we have defined $\hat{w}=\beta\nabla^2 w$ for convenience.

The conditions of vanishing bending moment and shearing stress are unaffected, as the displacement function is only indirectly approximated. We may therefore write

$$\hat{w}-\tilde{\beta}\left(\partial_s^2+\Theta'\partial_n\right)w=0\quad(\boldsymbol{x}\in\Upsilon) \tag{2.17a}$$

and

$$\partial_n\hat{w}+\tilde{\beta}\partial_s(\partial_s\partial_n-\Theta'\partial_s)w=0\quad(\boldsymbol{x}\in\Upsilon). \tag{2.17b}$$

The continuity condition (2.7) is also retained although this is inconsequential for the current work as a smooth boundary Υ has been assumed.

Our choice to take the primary vertical mode as being that which supports propagating waves means that the incident wave can be represented exactly in our approximation. It follows that the Sommerfeld radiation conditions imposed on the full-linear solution are also satisfied by our approximations, so that, for the floe and polynya problems, respectively,

$$r^{1/2}(\partial_r-\mathrm{i}k_0)\left(\phi-\phi^{(I)}\right)\to 0,\quad r^{1/2}(\partial_r-\mathrm{i}\kappa_0)\left(\psi-\psi^{(I)}\right)\to 0, \tag{2.18}$$

as $r\to\infty$, uniformly in θ.

2.3. *Corner singularity and joining conditions*

As fluid near the surface flows between the ice-covered and free-surface fluid regions it encounters a step caused by the draught of the ice. At this point the fluid must traverse the corner presented by the submerged portion of the ice edge and this results in a sharp change in the fluid velocity.

For a Laplacian flow around a fixed right-angled wedge, that is one that enforces Neumann conditions on both adjoining boundaries, it can be shown from an asymptotic analysis in the vicinity of the corner that the fluid's velocity has an order $-1/3$ singularity at this point. Analytical insight becomes more difficult when a thin-elastic plate condition is applied on one boundary but, by assuming the same order of singularity as in the fixed-wedge case, Williams & Porter (2009) elicited exponential convergence for two-dimensional problems involving partial ice cover with non-zero draught included. Since locally the corner created by the submerged portion of our floe or polynya will be the same as those studied by Williams & Porter (2009), we assume that

$$|\nabla\varphi|=O\left(\delta^{-1/3}\right)\quad\text{as }\delta\to 0, \tag{2.19}$$

where δ is the shortest distance of the field point from the corner created by the submerged ice edge, which is defined by the contour $\{\boldsymbol{x},z\,:\,\boldsymbol{x}\in\Upsilon,z=-d\}$. The incorporation of this singularity into the approximate solution is influential in determining its convergence rates and this motivates the technique we employ below.

Concomitantly, the vertical expansions (2.11*a*, *b*) partition the problem into the ice-covered and free-surface fluid regions, and it is therefore necessary to link the respective solutions at the boundary Υ, where the singular behaviour described above is relevant. Although it is inevitable from the partitioning that the approximate

solution will incur a discontinuity at the boundary of the water column located at $\boldsymbol{x} \in \Upsilon$, the joining conditions that will be outlined below ensure that continuity of fluid pressure and velocity will be recovered as the number of vertical modes is increased. The accuracy gained by using the natural vertical modes, relevant to the two particular surface conditions, far outweighs that lost by accepting approximations that possess a discontinuity at the interface between the free-surface and ice-covered fluid domains.

By introducing an auxiliary function u, which exists only beneath the ice edge $\boldsymbol{x} \in \Upsilon$, it was shown by Porter & Porter (2004) that the variational principle will assimilate the continuities

$$\varphi(\boldsymbol{x}_+, z) = \varphi(\boldsymbol{x}_-, z), \quad \partial_n \varphi(\boldsymbol{x}_+, z) = \partial_n \varphi(\boldsymbol{x}_-, z) = u(\boldsymbol{x}, z), \tag{2.20}$$

for $\boldsymbol{x} \in \Upsilon$ and $z \in (-h, -d)$, in the set of its natural conditions. This idea was then utilised by Bennetts *et al.* (2007) and in subsequent works, in conjunction with an expansion of the auxiliary function

$$u(\boldsymbol{x}, z) \approx \sum_{n=0}^{U} u_n(\boldsymbol{x}) \mathscr{U}_n(z), \tag{2.21}$$

where the functions $\mathscr{U}_n$ are known, to provide joining conditions for the approximate velocity potential. However, as noted by Bennetts *et al.* (2007), their choice of expansion set, namely $\mathscr{U}_n = \eta_n$, was not expected to be optimal and was restricted so that its dimension matched that of the surrounding domains, that is $U = N$.

The structure of u is dominated by the singularity (2.19) as $z \to -d$ and, although, of course, it is not essential, accounting for this feature when forming its approximation leads to enhanced convergence properties. To correctly embed the singularity we choose to set the modes $\mathscr{U}_n$ as

$$\mathscr{U}_n(z) = \mathscr{C}_{2n}^{(1/6)}\left(\frac{z+h}{H}\right) \quad (n = 0, \ldots, U), \tag{2.22}$$

where

$$\mathscr{C}_n^{(\alpha)}(t) = \frac{n!2^{2\alpha}(n+\alpha)\Gamma^2(\alpha)}{\pi\Gamma(n+2\alpha)H}(1-t^2)^{\alpha-1/2}C_n^{(\alpha)}(t), \tag{2.23}$$

in which Γ is the Gamma function and $C_n^{(\alpha)}$ is a Gegenbauer polynomial (see Abramowitz & Stegun 1964, § 22). This approach follows that of Williams & Porter (2009) who adopted an identical expansion. Weighted Gegenbauer polynomials were originally used as trial functions to capture the singularity in the fluid velocity field around a corner in a step on the seabed by Porter & Porter (2000).

Inserting this approximation into the variational principle results in the following joining conditions:

$$\boldsymbol{V}_0^{\mathrm{T}}\boldsymbol{\Phi} = \boldsymbol{V}_1^{\mathrm{T}}\boldsymbol{\Psi}, \tag{2.24a}$$

representing an approximate form of continuity of fluid pressure, and

$$\boldsymbol{A}_0(\partial_n\boldsymbol{\Phi}) = \boldsymbol{V}_0\boldsymbol{u}, \quad \boldsymbol{A}_1(\partial_n\boldsymbol{\Psi}) = \boldsymbol{V}_1\boldsymbol{u}, \tag{2.24b}$$

where the vector $\boldsymbol{u} = \boldsymbol{u}(s) = (u_0, \ldots, u_U)^{\mathrm{T}}$, which is an approximate version of continuity of fluid velocity. The matrix $\boldsymbol{A}_0$ that appears in these conditions, like $\boldsymbol{A}_1$, is square, of dimension $N+1$ and is defined by

$$\{\boldsymbol{A}_0\}_{j+1,i+1} = \int_{-h}^{0} \zeta_j \zeta_i \, \mathrm{d}z \quad (i, j = 0, \ldots, N). \tag{2.25}$$

This contrasts with the matrices $\boldsymbol{V}_0$ and $\boldsymbol{V}_1$ that are non-square and of size $(N+1)\times(U+1)$, as we allow for dimensions of the auxiliary function that are different to that of the approximate velocity potential. Their entries are given by the inner products

$$\{\boldsymbol{V}_0\}_{j+1,i+1} = \int_{-h}^{-d} \zeta_j \mathscr{U}_i \,\mathrm{d}z = \Gamma(\alpha)\left(\frac{2}{\mathrm{i}k_j H}\right)^{\alpha}(2i+\alpha)(-1)^i J_{2i+\alpha}(\mathrm{i}k_j H), \tag{2.26}$$

and

$$\{\boldsymbol{V}_1\}_{j+1,i+1} = \int_{-h}^{-d} \eta_j \mathscr{U}_i \,\mathrm{d}z = \Gamma(\alpha)\left(\frac{2}{\mathrm{i}\kappa_j H}\right)^{\alpha}(2i+\alpha)(-1)^i J_{2i+\alpha}(\mathrm{i}\kappa_j H) \tag{2.27}$$

(see Abramowitz & Stegun 1964, § 10), where J_n is the Bessel function of the first kind of order n and $\alpha = 1/6$. The freedom of having the dimensions N and U independent is important from a numerical standpoint when seeking accurate solutions and the technique for dealing with the non-square matrices in the solution process will be outlined in the following section.

3. Integro-differential equations

3.1. *Formulation*

The imposition of the joining conditions (2.24*a*, *b*) completes the new set of governing equations and our task is now to calculate the vectors of unknown functions $\boldsymbol{\Phi}$ and $\boldsymbol{\Psi}$ that define our approximation (2.11*a*, *b*) of the velocity potential, along with the corresponding approximation, w, of the displacement of the fluid–ice interface. During this process we will recover the vector $\boldsymbol{u}$, which defines the approximation of the auxiliary function u that represents horizontal fluid velocity beneath the ice edge. Although these functions exist in the horizontal plane only, their retrieval still constitutes a significant obstacle due to the arbitrary shape of the contour Υ that divides the ice-free and ice-covered fluid regions and prevents the application of a straightforward decomposition of the governing equation, which is possible for circular scatterers (e.g. Meylan & Squire 1996).

Before outlining the method that we will employ to obtain our approximation, it will be of algebraic benefit to rewrite the governing equations for the ice-covered fluid region in a single expression. Combining (2.15*a*, *b*) gives

$$\boldsymbol{B}_-\nabla^2\widetilde{\boldsymbol{\Psi}} + \boldsymbol{B}_+\widetilde{\boldsymbol{\Psi}} = \boldsymbol{0}, \tag{3.1}$$

where the $(N+3)$-length vector of unknowns $\widetilde{\boldsymbol{\Psi}} = \widetilde{\boldsymbol{\Psi}}(\boldsymbol{x}) = (\boldsymbol{\Psi}^{\mathrm{T}}(\boldsymbol{x}), w(\boldsymbol{x}), \hat{w}(\boldsymbol{x}))^{\mathrm{T}}$, and the $(N+3)$-square matrices $\boldsymbol{B}_-$ and $\boldsymbol{B}_+$ are defined by

$$\left.\begin{aligned}
&\{\boldsymbol{B}_-\}_{j,i} = \{\boldsymbol{A}_1\}_{j,i},\ \{\boldsymbol{B}_+\}_{j,i} = \left\{\boldsymbol{A}_1\boldsymbol{K}_1^2 - \boldsymbol{C}_1\boldsymbol{o}\boldsymbol{o}^{\mathrm{T}}\boldsymbol{K}_1\boldsymbol{S}_1\right\}_{j,i} \quad (i,j=1,\ldots,N+1),\\
&\{\boldsymbol{B}_-\}_{N+j,N+j} = 1 \ \ (j=2,3), \quad \{\boldsymbol{B}_+\}_{N+2,N+3} = -1/\beta,\\
&\{\boldsymbol{B}_+\}_{N+3,j} = -\{\boldsymbol{o}^{\mathrm{T}}\boldsymbol{C}_1\}_{1,j}\ (j=1,\ldots,N+1), \quad \{\boldsymbol{B}_+\}_{N+3,N+2} = 1-\sigma d,
\end{aligned}\right\} \tag{3.2}$$

with all unspecified entries being zero. It is possible to simplify expression (3.1) by diagonalising $\boldsymbol{B}_-^{-1}\boldsymbol{B}_+$, to produce

$$\nabla^2\widetilde{\boldsymbol{\Psi}} + \boldsymbol{C}\widetilde{\boldsymbol{K}}^2\boldsymbol{C}^{-1}\widetilde{\boldsymbol{\Psi}} = \boldsymbol{0}. \tag{3.3}$$

The matrices $\widetilde{\boldsymbol{K}}$ and $\boldsymbol{C}$ are defined by $\widetilde{\boldsymbol{K}} = \lceil \kappa_0, \ldots, \kappa_N, \kappa_{-1}, \kappa_{-2} \rfloor$ and

$$\left.\begin{array}{l} \{\boldsymbol{C}\}_{n,n} = 1, \quad \{\boldsymbol{C}\}_{N+2,n} = \sigma^{-1}\kappa_{n-1}\sinh(\kappa_{n-1}H), \quad \{\boldsymbol{C}\}_{N+3,n} = -\beta\kappa_{n-1}^2\{\boldsymbol{C}\}_{N+2,n}, \\ \{\boldsymbol{C}\}_{n,N+i} = \{\boldsymbol{c}(\kappa_{-i})\}_n, \quad \{\boldsymbol{C}\}_{N+2,N+i} = 1, \quad \{\boldsymbol{C}\}_{N+3,N+i} = -\beta\kappa_{-i}^2 \end{array}\right\} \tag{3.4}$$

for $n = 1, \ldots, N+1$ and $i = 2, 3$. Appearing in the definition of these matrices are the quantities κ_{-i} $(i = 1, 2)$, which are the roots κ of the quartic equation

$$(\beta\kappa^4 + 1 - \sigma d) + \beta \boldsymbol{o}^{\mathrm{T}}\boldsymbol{C}_1\boldsymbol{A}_1^{-1}\big(\boldsymbol{K}_1^2 + \kappa^2\boldsymbol{I}\big)\boldsymbol{K}_1\boldsymbol{S}_1\boldsymbol{o} = 0, \tag{3.5}$$

which exist in the upper-half complex plane, and also the vector $\boldsymbol{c} = \boldsymbol{c}(\kappa)$ that is calculated from

$$\boldsymbol{A}_1\boldsymbol{c} + \beta\big(\boldsymbol{K}_1^2 + \kappa^2\boldsymbol{I}\big)\boldsymbol{K}_1\boldsymbol{S}_1\boldsymbol{o} = \boldsymbol{0}, \tag{3.6}$$

where $\boldsymbol{I}$ is the identity matrix of size $N+1$. The motion associated to the κ_{-i} and the $\boldsymbol{c}(\kappa_{-i})$ $(i = 1, 2)$ recreates the oscillatory-evanescent waves that are supported by ice-covered fluid and corresponds to the two modes left absent from the approximation due to linear dependence (see Bennetts *et al.* 2007).

We now recast the governing equations in the free-surface and ice-covered fluid regions as sets of integral representations from which it is possible to derive a solution method. Application of matrices of Green's functions along with Green's theorem in the plane turn (2.14) and (3.3), respectively, into

$$\epsilon\boldsymbol{\Phi}(\boldsymbol{x}) = \boldsymbol{\Phi}^{(I)}(\boldsymbol{x}) - \frac{1}{4\mathrm{i}}\int_{\Upsilon}\{(\partial_N\boldsymbol{H}_0(R))\boldsymbol{\Phi}(\boldsymbol{X}) - \boldsymbol{H}_0(R)(\partial_N\boldsymbol{\Phi}(\boldsymbol{X}))\}\,\mathrm{d}S \quad (\boldsymbol{x} \in \Omega_0), \tag{3.7a}$$

and

$$\epsilon\widetilde{\boldsymbol{\Psi}}(\boldsymbol{x}) = \frac{1}{4\mathrm{i}}\int_{\Upsilon}\{(\partial_N\boldsymbol{H}_1(R))\widetilde{\boldsymbol{\Psi}}(\boldsymbol{X}) - \boldsymbol{H}_1(R)(\partial_N\widetilde{\boldsymbol{\Psi}}(\boldsymbol{X}))\}\,\mathrm{d}S \quad (\boldsymbol{x} \in \Omega_1), \tag{3.7b}$$

for the floe problem, or

$$\epsilon\boldsymbol{\Phi}(\boldsymbol{x}) = \frac{1}{4\mathrm{i}}\int_{\Upsilon}\{(\partial_N\boldsymbol{H}_0(R))\boldsymbol{\Phi}(\boldsymbol{X}) - \boldsymbol{H}_0(R)(\partial_N\boldsymbol{\Phi}(\boldsymbol{X}))\}\,\mathrm{d}S \quad (\boldsymbol{x} \in \Omega_0), \tag{3.8a}$$

and

$$\epsilon\widetilde{\boldsymbol{\Psi}}(\boldsymbol{x}) = \widetilde{\boldsymbol{\Psi}}^{(I)}(\boldsymbol{x}) - \frac{1}{4\mathrm{i}}\int_{\Upsilon}\{(\partial_N\boldsymbol{H}_1(R))\widetilde{\boldsymbol{\Psi}}(\boldsymbol{X}) - \boldsymbol{H}_1(R)(\partial_N\widetilde{\boldsymbol{\Psi}}(\boldsymbol{X}))\}\,\mathrm{d}S \quad (\boldsymbol{x} \in \Omega_1), \tag{3.8b}$$

for the polynya problem, where the quantity ϵ is defined as $\epsilon = (1/2)\,(\boldsymbol{x} \in \Upsilon)$ and $\epsilon = 1$ $(\boldsymbol{x} \notin \Upsilon)$. In these equations, the arclength S and normal derivative ∂_N on Υ are with respect to $\boldsymbol{X}$.

The above expressions give the unknown functions in their respective domains in terms of convolutions involving themselves and matrices of Green's functions and their normal derivatives, where the integrals are over the contour Υ. The matrices of Green's functions, namely $\boldsymbol{H}_0$ and $\boldsymbol{H}_1$, are defined as

$$\boldsymbol{H}_0(R) = \lceil H_0(k_0R), \ldots, H_0(k_NR) \rfloor, \tag{3.9a}$$

and

$$\boldsymbol{H}_1(R) = \boldsymbol{C}\lceil H_0(\kappa_0R), \ldots, H_0(\kappa_NR), H_0(\kappa_{-1}R), H_0(\kappa_{-2}R)\rfloor\boldsymbol{C}^{-1}, \tag{3.9b}$$

where H_0 denotes the Hankel function of the first kind of order 0. Each Green's function represents circular waves emanating from a source point $\boldsymbol{X}$, so that they

depend only on the Cartesian distance of the field point $\boldsymbol{x}$ from the source point, that is $R = |\boldsymbol{x} - \boldsymbol{X}|$. In (3.7*a*), the incident wave for the floe problem, $\phi^{(I)}$, appears through the vector $\boldsymbol{\Phi}^{(I)} = (\phi^{(I)}, 0, \ldots, 0)^{\mathrm{T}}$, which is of length $N+1$, and likewise in (3.8*b*) the incident wave for the polynya problem, $\psi^{(I)}$, appears through $\widetilde{\boldsymbol{\Psi}}^{(I)} = \boldsymbol{C}(\psi^{(I)}, 0, \ldots, 0)^{\mathrm{T}}$, which is of length $N+3$.

Allowing the field point $\boldsymbol{x}$ to tend to the boundary Υ from the respective free-surface and ice-covered fluid domains in (3.7*a*, *b*) and (3.8*a*, *b*) produces a set of integral equations. As these integral equations are posed on Υ we may implement the free-edge conditions (2.17*a*, *b*) to eliminate the unknowns $\hat{w}$ and $\partial_n \hat{w}$ in favour of terms involving w and $\partial_n w$, although this leaves us with a set of integro-differential equations. These integro-differential equations may be written as

$$\frac{1}{2}\boldsymbol{\Phi} = \boldsymbol{\Phi}^{(I)} - \frac{1}{4\mathrm{i}}\int_{\Upsilon} \{(\partial_N \boldsymbol{H}_0)\boldsymbol{\Phi} - \boldsymbol{H}_0(\partial_N \boldsymbol{\Phi})\}\,\mathrm{d}S \quad (\boldsymbol{x} \in \Upsilon), \tag{3.10a}$$

and

$$\boldsymbol{E}_1 \widehat{\boldsymbol{\Psi}} = \frac{1}{4\mathrm{i}}\int_{\Upsilon} \{\boldsymbol{F}_1 \widehat{\boldsymbol{\Psi}} - \boldsymbol{G}_1(\partial_N \boldsymbol{\Psi})\}\,\mathrm{d}S \quad (\boldsymbol{x} \in \Upsilon), \tag{3.10b}$$

for the floe problem, where $\widehat{\boldsymbol{\Psi}} = (\boldsymbol{\Psi}^{\mathrm{T}}, w, \partial_n w)^{\mathrm{T}}$. Analogous expressions are produced for the polynya problem. The matrices $\boldsymbol{E}_1 = \boldsymbol{E}_1(R)$ and $\boldsymbol{F}_1 = \boldsymbol{F}_1(R)$ are size $(N+3)$-square and are differential operators defined by

$$\{\boldsymbol{E}_1\}_{j,j} = \tfrac{1}{2}(j = 1, \ldots, N+2), \quad \{\boldsymbol{E}_1\}_{N+3,N+2} = \frac{\tilde{\beta}}{2}\partial_s^2, \tag{3.11}$$

$$\{\boldsymbol{E}_1\}_{N+3,N+3} = \frac{\tilde{\beta}}{2}\Theta', \quad \{\boldsymbol{F}_1\}_{j,i} = \{\partial_N \boldsymbol{H}_1\}_{j,i} \ \ (j = 1, \ldots, N+3, i = 1, \ldots, N+1), \tag{3.12}$$

$$\{\boldsymbol{F}_1\}_{j,N+2} = \{\partial_N \boldsymbol{H}_1\}_{j,N+2} + \tilde{\beta}\{(\partial_N \boldsymbol{H}_1)\partial_S^2 - \boldsymbol{H}_1 \partial_S \Theta' \partial_S\}_{j,N+3} \ \ (j = 1, \ldots, N+3), \tag{3.13}$$

and

$$\{\boldsymbol{F}_1\}_{j,N+3} = \tilde{\beta}\{\Theta' \partial_N \boldsymbol{H}_1 + \boldsymbol{H}_1 \partial_S^2\}_{j,N+3} - \{\boldsymbol{H}_1\}_{j,N+2} \ \ (j = 1, \ldots, N+3). \tag{3.14}$$

The matrix $\boldsymbol{G}_1 = \boldsymbol{G}_1(R)$ is size $(N+3) \times (N+1)$ and is defined as

$$\{\boldsymbol{G}_1\}_{j,i} = \{\boldsymbol{H}_1\}_{j,i} \ \ (j = 1, \ldots, N+3, i = 1, \ldots, N+1). \tag{3.15}$$

The number of unknowns can be reduced further still by applying the second of the joining conditions (2.24*b*) to replace $\partial_n \boldsymbol{\Psi}$ and $\partial_n \boldsymbol{\Phi}$ by $\boldsymbol{u}$ and leaves

$$\frac{1}{2}\boldsymbol{\Phi} = \boldsymbol{\Phi}^{(I)} - \frac{1}{4\mathrm{i}}\int_{\Upsilon} \{(\partial_N \boldsymbol{H}_0)\boldsymbol{\Phi} - \boldsymbol{H}_0 \boldsymbol{A}_0^{-1} \boldsymbol{V}_0 \boldsymbol{u}\}\,\mathrm{d}S \quad (\boldsymbol{x} \in \Upsilon), \tag{3.16a}$$

and

$$\boldsymbol{E}_1 \widehat{\boldsymbol{\Psi}} = \frac{1}{4\mathrm{i}}\int_{\Upsilon} \{\boldsymbol{F}_1 \widehat{\boldsymbol{\Psi}} - \boldsymbol{G}_1 \boldsymbol{A}_1^{-1} \boldsymbol{V}_1 \boldsymbol{u}\}\,\mathrm{d}S \quad (\boldsymbol{x} \in \Upsilon), \tag{3.16b}$$

for the floe problem and similarly for the polynya problem.

3.2. *Solution via the Galerkin technique*

Our objective of determining the wave-scattering properties of three-dimensional geometries has now been reduced to finding the solutions to two classes of finite systems of one-dimensional integro-differential equations. In order to solve these

integro-differential systems, we will make use of the Galerkin technique. This entails the expansion of the unknowns in a set of chosen trial functions, $\{\chi_p : p \in \mathbb{Z}\}$ say, and the truncation of these expressions, and we write

$$[\boldsymbol{\Phi}]_\Upsilon \equiv \boldsymbol{p}_0(s) \approx \frac{1}{2\gamma} \sum_{m=-M}^{M} \boldsymbol{p}_{0,m} \chi_m(s), \quad [\boldsymbol{\Psi}]_\Upsilon \equiv \boldsymbol{p}_1(s) \approx \frac{1}{2\gamma} \sum_{m=-M}^{M} \boldsymbol{p}_{1,m} \chi_m(s), \quad (3.17a)$$

and

$$[\widehat{\boldsymbol{\Psi}}]_\Upsilon \equiv \boldsymbol{q}_1(s) \approx \frac{1}{2\gamma} \sum_{m=-M}^{M} \boldsymbol{q}_{1,m} \chi_m(s), \quad \boldsymbol{u}(s) \approx \frac{1}{2\gamma} \sum_{m=-M}^{M} \boldsymbol{u}_m \chi_m(s), \quad (3.17b)$$

where M is an arbitrary positive constant that provides desired accuracy. Whereupon, inner products of the equations are taken with each of the trial functions in turn to convert the problem into a matrix system. As the boundary Υ has been assumed to be smooth, the unknown functions are clearly periodic and it is appropriate to use exponential functions for our expansions, so that

$$\chi_m = \chi_m(s) = \mathrm{e}^{\mathrm{i}\mu_m s}, \quad \mu_m = \frac{m\pi}{\gamma} \quad (m = -M, \ldots, M). \quad (3.18)$$

The case in which piece-wise continuous boundaries are admitted produces some interesting and non-trivial features in the solution that will be investigated in a future work.

Implementing the Galerkin technique on our floe problem (3.16*a*, *b*) and the analogous polynya problem, using the above approximations and choice of trial functions, and noting that the tangential derivatives of the displacement functions may be evaluated explicitly, leads to a linear system of equations for the unknown constant vectors $\boldsymbol{p}_{0,m}$, $\boldsymbol{q}_{1,m}$ (containing $\boldsymbol{p}_{1,m}$) and $\boldsymbol{u}_m$ $(m = -M, \ldots, M)$. This system may be expressed as

$$\tfrac{1}{2}\widehat{\boldsymbol{p}}_0 = \widehat{\boldsymbol{f}}_0 - \widehat{\boldsymbol{F}}_0\widehat{\boldsymbol{p}}_0 + \widehat{\boldsymbol{G}}_0\widehat{\boldsymbol{u}} \quad (3.19a)$$

and

$$\widehat{\boldsymbol{E}}_1\widehat{\boldsymbol{q}}_1 = \widehat{\boldsymbol{F}}_1\widehat{\boldsymbol{q}}_1 - \widehat{\boldsymbol{G}}_1\widehat{\boldsymbol{u}}, \quad (3.19b)$$

for the floe problem, and

$$\tfrac{1}{2}\widehat{\boldsymbol{p}}_0 = \widehat{\boldsymbol{F}}_0\widehat{\boldsymbol{p}}_0 - \widehat{\boldsymbol{G}}_0\widehat{\boldsymbol{u}} \quad (3.20a)$$

and

$$\widehat{\boldsymbol{E}}_1\widehat{\boldsymbol{q}}_1 = \widehat{\boldsymbol{f}}_1 - \widehat{\boldsymbol{F}}_1\widehat{\boldsymbol{q}}_1 + \widehat{\boldsymbol{G}}_1\widehat{\boldsymbol{u}}, \quad (3.20b)$$

for the polynya problem. Here the length $(2M+1)(N+1)$ vector $\widehat{\boldsymbol{p}}_0$, length $(2M+1)(N+3)$ vector $\widehat{\boldsymbol{q}}_1$ (containing the length $(2M+1)(N+1)$ vector $\widehat{\boldsymbol{p}}_1$) and length $(2M+1)(U+1)$ vector $\widehat{\boldsymbol{u}}$ amalgamate the respective unknowns, such that

$$\widehat{\boldsymbol{p}}_i = \begin{pmatrix} \boldsymbol{p}_{i,-M} \\ \vdots \\ \boldsymbol{p}_{i,M} \end{pmatrix} \quad (i = 0, 1), \quad \widehat{\boldsymbol{q}}_1 = \begin{pmatrix} \boldsymbol{q}_{1,-M} \\ \vdots \\ \boldsymbol{q}_{1,M} \end{pmatrix}, \quad \widehat{\boldsymbol{u}} = \begin{pmatrix} \boldsymbol{u}_{-M} \\ \vdots \\ \boldsymbol{u}_M \end{pmatrix}. \quad (3.21)$$

The size $(2M+1)(N+1)$-square matrix $\widehat{\boldsymbol{F}}_0$, size $(2M+1)(N+1) \times (2M+1)(U+1)$ matrix $\widehat{\boldsymbol{G}}_0$, size $(2M+1)(N+3)$-square matrices $\widehat{\boldsymbol{E}}_1$ and $\widehat{\boldsymbol{F}}_1$, and size $(2M+1)(N+3) \times (2M+1)(U+1)$ matrix $\widehat{\boldsymbol{G}}_1$ collect together the various inner products, with their

block entries given by

$$\{\widehat{\boldsymbol{F}}_0\}_{j,i} = \langle\langle \partial_N \boldsymbol{H}_0, \chi_i, \chi_j\rangle\rangle, \quad \{\widehat{\boldsymbol{G}}_0\}_{j,i} = \left\langle\left\langle \boldsymbol{H}_0\boldsymbol{A}_0^{-1}\boldsymbol{V}_0, \chi_i, \chi_j\right\rangle\right\rangle, \tag{3.22}$$

$$\{\widehat{\boldsymbol{E}}_1\}_{j,i} = \langle \boldsymbol{E}_1\chi_i, \chi_j\rangle, \quad \{\widehat{\boldsymbol{F}}_1\}_{j,i} = \langle\langle \boldsymbol{F}_1, \chi_i, \chi_j\rangle\rangle, \quad \{\widehat{\boldsymbol{G}}_1\}_{j,i} = \left\langle\left\langle \boldsymbol{G}_1\boldsymbol{A}_1^{-1}\boldsymbol{V}_1, \chi_i, \chi_j\right\rangle\right\rangle, \tag{3.23}$$

for $i, j = -M, \ldots, M$, using the notation

$$\langle f, g\rangle = \frac{1}{2\gamma}\int_{-\gamma}^{\gamma} f(s)\overline{g}(s)\,\mathrm{d}s, \quad \langle\langle F, g, h\rangle\rangle = \frac{1}{8\gamma \mathrm{i}}\int_{-\gamma}^{\gamma}\int_{-\gamma}^{\gamma} F(s|S)g(s)\overline{h}(S)\,\mathrm{d}S\,\mathrm{d}s, \tag{3.24}$$

and where the brackets $\{\cdot\}$ are used in these instances to indicate a relevant block entry. Forcing is provided by inner products of the incident waves, which are contained in the vectors

$$\widehat{\boldsymbol{f}}_0 = \left(\langle \boldsymbol{\Phi}^{(I)}, \chi_{-M}\rangle^{\mathrm{T}}, \ldots, \langle \boldsymbol{\Phi}^{(I)}, \chi_M\rangle^{\mathrm{T}}\right)^{\mathrm{T}}, \tag{3.25}$$

in (3.19*a*) for the floe problem, and

$$\widehat{\boldsymbol{f}}_1 = \left(\langle \widetilde{\boldsymbol{\Psi}}^{(I)}, \chi_{-M}\rangle^{\mathrm{T}}, \ldots, \langle \widetilde{\boldsymbol{\Psi}}^{(I)}, \chi_M\rangle^{\mathrm{T}}\right)^{\mathrm{T}}, \tag{3.26}$$

in (3.20*b*) for the polynya problem.

It is well known that two-dimensional Green's functions contain a logarithmic singularity at the point at which the source and field points coincide and this issue requires special attention when constructing numerical routines to find the entries of the above matrices. Specifically, the singularities occur in the Hankel functions, with

$$H_0(kR) \sim \frac{2\mathrm{i}}{\pi}\ln(R) \quad (R \to 0). \tag{3.27}$$

It is a standard technique when considering such problems to subtract the singular term from the integral to leave a bounded function amenable to numerical integration, and evaluate the contribution of the logarithm analytically. In order to do this, it is of great benefit to encapsulate the singularity in a more appealing function, by noting that

$$\ln(R) - \ln\left(\frac{|1 - \mathrm{e}^{\mathrm{i}\mu_1(s-S)}|}{\mu_1}\right) \to 0 \quad (R \to 0), \tag{3.28}$$

so that the value of the integral containing the singularity is independent of the shape of Υ. Due to our assumption of a smooth boundary Υ, the normal derivative $\partial_N H(kR)$ is bounded as the contour Υ is traversed and its limit may be derived in a straightforward manner, meaning that the integrals it appears in are conducive to direct numerical evaluation.

For the floe problem, the simple rearrangements of (3.19*a*, *b*)

$$\widehat{\boldsymbol{p}}_0 = \left(\tfrac{1}{2}\boldsymbol{I} + \widehat{\boldsymbol{F}}_0\right)^{-1}(\widehat{\boldsymbol{f}}_0 + \widehat{\boldsymbol{G}}_0\widehat{\boldsymbol{u}}), \quad \widehat{\boldsymbol{q}}_1 = -(\widehat{\boldsymbol{E}}_1 - \widehat{\boldsymbol{F}}_1)^{-1}\widehat{\boldsymbol{G}}_1\widehat{\boldsymbol{u}}, \tag{3.29}$$

where now $\boldsymbol{I}$ is used to denote the identity matrix of dimension $(2M+1)(N+1)$, allow the vector $\widehat{\boldsymbol{p}}_0$ to be expressed in terms of the forcing term $\widehat{\boldsymbol{f}}_0$ and the vector of unknowns $\widehat{\boldsymbol{u}}$ and the vector $\widehat{\boldsymbol{q}}_1$ to be expressed in terms of $\widehat{\boldsymbol{u}}$ alone. It only remains to enforce the first of the joining conditions (2.24*a*), and this is achieved via the Galerkin technique, so that $\boldsymbol{V}_0^{\mathrm{T}}\boldsymbol{p}_{0,m} = \boldsymbol{V}_1^{\mathrm{T}}\boldsymbol{p}_{1,m}$ $(m = -M, \ldots, M)$. Collecting these conditions together and substituting for $\widehat{\boldsymbol{p}}_0$ and $\widehat{\boldsymbol{p}}_1$ using (3.29) we have

$$\widehat{\boldsymbol{V}}_0\left(\tfrac{1}{2}\boldsymbol{I} + \widehat{\boldsymbol{F}}_0\right)^{-1}(\widehat{\boldsymbol{f}}_0 + \widehat{\boldsymbol{G}}_0\widehat{\boldsymbol{u}}) = -\widehat{\boldsymbol{V}}_1[(\widehat{\boldsymbol{E}}_1 - \widehat{\boldsymbol{F}}_1)^{-1}\widehat{\boldsymbol{G}}_1]_{\widehat{\boldsymbol{p}}_1}\widehat{\boldsymbol{u}}, \tag{3.30}$$

where $\widehat{\boldsymbol{V}}_i$ ($i=0, 1$) is a $(2M+1)(U+1)\times(2M+1)(N+1)$ block-diagonal matrix with entries $\boldsymbol{V}_i$ and $[\cdot]_{\widehat{p}_1}$ denotes the restriction of a matrix to only those rows pertaining to $\widehat{\boldsymbol{p}}_1$, that is leaving out every $(N+2)$th and $(N+3)$th row. The linear system of $(2M+1)(U+1)$ equations represented by this equation may be manipulated in a straightforward manner to calculate the vector $\widehat{\boldsymbol{u}}$, from which we may obtain all unknowns on Υ using (3.29) and expansions (3.17) and subsequently in the entire horizontal domain using expressions (3.7*a*, *b*), thus completing the solution process. An identical method is applied to solve the polynya problem.

4. Far-field representation and energy conservation

A region of particular interest in wave-scattering problems is the far-field ($r\to\infty$), as analysis of the diffracted field there allows us to ascertain some of the key properties of the scattering source, which in our case is either the floe or the polynya. Therefore, let the diffracted part of solution be $\phi^{(D)}=\phi^{(D)}(r,\theta,z)$ for the floe problem, where $\phi^{(D)}=\phi-\phi^{(I)}$, and similarly $\psi^{(D)}=\psi^{(D)}(r,\theta,z)$ for the polynya problem, where $\psi^{(D)}=\psi-\psi^{(I)}$. From the Sommerfeld radiation conditions (2.18), we may deduce that the most slowly decaying part of the outgoing wave in each problem has the form

$$\phi^{(D)}\sim\sqrt{\frac{2}{\pi k_0 r}}\mathrm{e}^{\mathrm{i}k_0(r-\pi/4)}\mathscr{A}_0(\theta)\zeta_0(z),\quad \psi^{(D)}\sim\sqrt{\frac{2}{\pi\kappa_0 r}}\mathrm{e}^{\mathrm{i}\kappa_0(r-\pi/4)}\mathscr{A}_1(\theta)\eta_0(z),\tag{4.1}$$

as $r\to\infty$, where $\mathscr{A}_0$ and $\mathscr{A}_1$ are known as diffracted far-field amplitudes (DFFAs).

In order to find accessible expressions for the DFFAs, note that when the source point is on the contour Υ and the field point is far away from it, the following representations for the functions $\boldsymbol{H}_0$ and $\boldsymbol{H}_1$ hold:

$$\boldsymbol{H}_0(R)\sim\sqrt{\frac{2}{\pi k_0 r}}\widetilde{\boldsymbol{I}}_0\sum_{m\in\mathbb{Z}}\tilde{J}_{0,m}(\boldsymbol{X})\mathrm{e}^{\mathrm{i}m\theta},\quad \boldsymbol{H}_1(R)\sim\sqrt{\frac{2}{\pi\kappa_0 r}}\boldsymbol{C}\widetilde{\boldsymbol{I}}_1\boldsymbol{C}^{-1}\sum_{m\in\mathbb{Z}}\tilde{J}_{1,m}(\boldsymbol{X})\mathrm{e}^{\mathrm{i}m\theta},\tag{4.2}$$

for $|\boldsymbol{x}|\to\infty$ and $\boldsymbol{X}\in\Upsilon$, where the functions

$$\tilde{J}_{0,m}(\boldsymbol{X})\equiv J_m(k_0\varrho)\mathrm{e}^{-\mathrm{i}m(\vartheta-\pi/2)},\quad \tilde{J}_{1,m}(\boldsymbol{X})\equiv J_m(\kappa_0\varrho)\mathrm{e}^{-\mathrm{i}m(\vartheta-\pi/2)},\tag{4.3}$$

contain ϱ and ϑ, which are the source equivalents of r and θ, respectively. The matrix $\widetilde{\boldsymbol{I}}_i$ is size $(N+1)$-square for $i=0$ and $(N+3)$-square for $i=1$, and both have a unit entry in the top-left position and zeros elsewhere.

Substituting these representations into the integral expressions (3.7*a*) and (3.8*b*) for the respective floe and polynya problems, the DFFAs are found to be

$$\mathscr{A}_0(\theta)=\frac{1}{4\mathrm{i}}\sum_{m\in\mathbb{Z}}\int_\Upsilon\{\tilde{J}_{0,m}(\boldsymbol{X})\big(\partial_N\phi_0(\boldsymbol{X})\big)-\big(\partial_N\tilde{J}_{0,m}(\boldsymbol{X})\big)\phi_0(\boldsymbol{X})\}\,\mathrm{d}S\;\mathrm{e}^{\mathrm{i}m\theta},\tag{4.4a}$$

and

$$\mathscr{A}_1(\theta)=\frac{1}{4\mathrm{i}}\boldsymbol{c}_1^{\mathrm{T}}\sum_{m\in\mathbb{Z}}\int_\Upsilon\{\tilde{J}_{1,m}(\boldsymbol{X})\big(\partial_N\widetilde{\boldsymbol{\Psi}}(\boldsymbol{X})\big)-\big(\partial_N\tilde{J}_{1,m}(\boldsymbol{X})\big)\widetilde{\boldsymbol{\Psi}}(\boldsymbol{X})\}\,\mathrm{d}S\;\mathrm{e}^{\mathrm{i}m\theta},\tag{4.4b}$$

where $\boldsymbol{c}_1=\{\boldsymbol{C}^{-1}\}_{1,n}$ for $n=1,\ldots,N+3$. These quantities may be calculated once the unknown functions have been obtained on the interface Υ using the theory presented in § 3.

Whilst the functions $\mathscr{A}_0$ and $\mathscr{A}_1$ define the angular distribution of the diffracted wave in the far-field, it is often informative rather to possess a single value to assess the

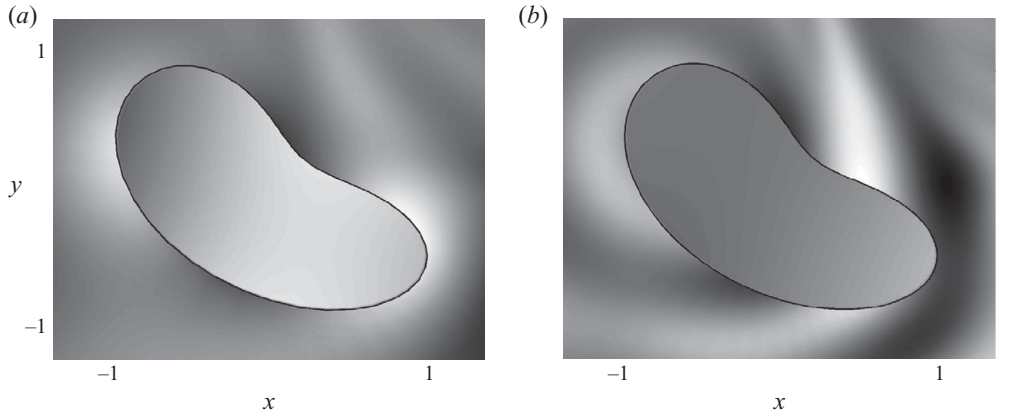

FIGURE 3. The displacement of crooked egg-shaped floes and the surrounding diffracted wave fields. The incident wave propagates along the x-axis from $x \to -\infty$ and the (non-dimensional) free-surface wavelength $\lambda = 2\pi/k_0$ is 2 in (a) and 1 in (b).

relative magnitude of the outgoing wave. Therefore, consider the so-called scattering cross-sections (SCCs)

$$\mathscr{S}_0 = \frac{1}{2\pi}\int_0^{2\pi} |\mathscr{A}_0(\theta)|^2 \,\mathrm{d}\theta, \quad \mathscr{S}_1 = \frac{1}{2\pi}\int_0^{2\pi} |\mathscr{A}_1(\theta)|^2 \,\mathrm{d}\theta, \tag{4.5}$$

which are non-dimensional quantities that are proportional to the ratio of the flux of the diffracted wave to the flux of the incident wave across a unit length taken parallel to one of its wave crests (see Norris & Vemula 1995, for further information).

Applying Green's theorem to the pair $(\phi_0, \overline{\phi}_0)$ for the floe problem or $(\psi_0, \overline{\psi}_0)$ for the polynya problem leads to the identities

$$\mathscr{S}_0 = \mathrm{Re}\{\mathscr{A}_0(\tau)\}, \quad \mathscr{S}_1 = \mathrm{Re}\{\mathscr{A}_1(\tau)\}. \tag{4.6}$$

This is a familiar result in many applications and is conventionally known as the optical theorem. In a study closely related to our own, that of wave scattering by finite straight-line cracks in floating ice sheets, the optical theorem has also been obtained (Porter & Evans 2007). Although the identities given in (4.6) ensure that energy conservation is obeyed and thus serve as a useful numerical check, it is important to realise that they apply for all dimensions N of the vertical expansions (2.11a, b) and hence do not imply that convergence has been achieved with respect to this approximation.

5. Numerical results

The numerical results that are presented in this section are intended to demonstrate the efficiency of the solution method outlined in this work and also to justify the need to model the shape of a scattering source. Due to the wealth of parameters that are at our disposal during the numerical investigation, for the results shown here the thickness of the ice will be set as $D = 1\,\mathrm{m}$ and the depth of the free-surface fluid as $h = 20\,\mathrm{m}$, as these are typical values and are not quantities associated with our primary interest, which is the shape of the floe or polynya.

Figures 3 and 4 display the wave elevation within the floe or polynya at the instant $t = 0$, along with the surrounding diffracted wave field. The crooked egg shape of the

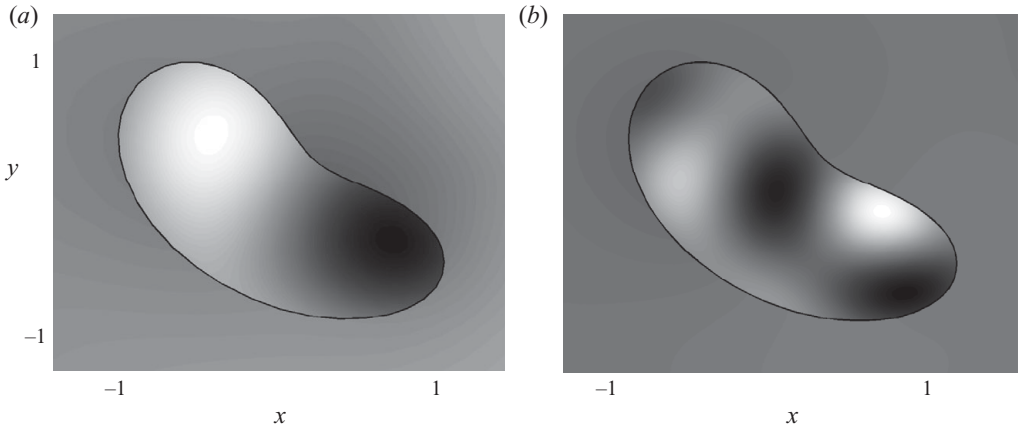

FIGURE 4. As in figure 3 but for polynyas.

scattering source is defined parametrically by

$$x = A(\xi)\cos(\xi),\ y = A(\xi)\sin(\xi);\ A(\xi) = a_0(\cos^3(\xi) + \sin^3(\xi)) \quad (0 < \xi < \pi). \tag{5.1}$$

This curve is overlaid on the plots with thick black lines and is chosen to be asymmetric with respect to the incident wave that propagates along the x-axis from $x \to -\infty$ ($\tau = 0$). The responses of both the floe and the polynya to two incident wavelengths are shown. In figures 3(a) and 4(a), $\lambda = 2\pi/k_0 = 2$, and in figures 3(b) and 4(b), $\lambda = 1$, where the horizontal scale has been non-dimensionalised with respect to a length scale of the scatterer ($\approx$30 m, so $a_0 \approx 1.5$). The above choice means that the corresponding panels of figures 3 and 4 are consistent in terms of frequency but differ in terms of incident wavelength, as ice cover is known to elongate waves.

The results given here are taken to be converged. To quantify this, consecutive values of the L_2 relative error of the wave elevation at the boundary Υ were made to diminish to $O(10^{-3})$ as the respective dimensions of the expansion of the velocity potential in vertical modes (N), the expansion of the fluid velocity beneath the ice edge in Gegenbauer polynomials (U) and the Galerkin expansion (M) were increased. For the floe forced by the longer incident wave this required ten vertical modes, three Gegenbauer polynomials and fifteen trial functions in the Galerkin expansions. When the floe is forced by the shorter wave, the only significant change in terms of dimensional requirement is to the Galerkin expansion, which demands twice the number of trial functions. The polynya problems of figure 4 necessitate slightly fewer terms to be used to gain the same degree of accuracy as their floe problem counterparts but this is interpreted as simply being due to the issue of differing incident wavelengths.

It is interesting to note the behaviour of the wave fields in the situations depicted in these figures. For the floe problems of figure 3, there is a significant influence of the shape of the scatterer on the diffracted wave. In particular, there is prominent activity in the vicinity of the floe where it is concave (approximately $0 < \xi, \theta < \pi/2$) and it can also be seen that the floe shape bends the wave, although the circular waves (4.1) that radiate away into the far-field are not in evidence at this close range. The majority of the wave energy that is scattered appears to travel in a direction close to that of the incident wave but altered slightly downwards. Of course, the behaviours described are more accentuated for the higher frequency. The wave elevation in the

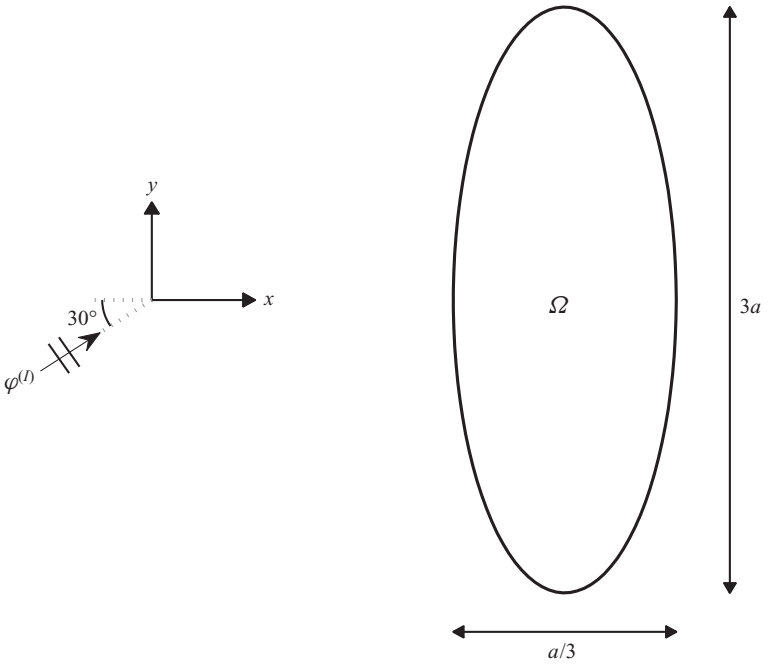

FIGURE 5. A schematic of the problem in the horizontal plane considered in figures 6–11 for the case in which the floe ($\Omega = \Omega_1$) or polynya ($\Omega = \Omega_0$) is elliptical and stretched in the y direction.

polynyas takes the form of peaks and troughs, and in the shorter wavelength case, where a number of these features are excited, there is marked rotation in their shape across the pool.

Let us now turn to the question of how differently shaped floes and polynyas diffract incident waves. For this purpose we consider four shapes of scatterers, one circular of radius $a = 50$ m, the crooked egg shape of figures 3 and 4, and two ellipses, representing circles stretched in directions parallel to the x- and y-axis, respectively. All of the shapes are scaled so that the area of the horizontal plane they occupy is consistent. In the case of the ellipses, the stretch factor is 3 and a schematic of the problem posed by the latter of these is shown in figure 5.

In figures 6 and 7, the DFFAs given in (4.4a, b) are shown for each of these shapes, where the incident wave angle is $\tau = 30^\circ$ and for two wavelengths $\lambda = 1$ and 2, which have been non-dimensionalised with respect to the radius a. It is striking that there is much variation of this far-field response between the different shapes for both the floe and the polynya problems and for both wavelengths. Although some consistent traits are evident in these results, it is not often possible to prescribe a behaviour to a particular shape, which is a product of the complicated nature of the phenomena being modelled.

In almost all situations, as would be expected from previous studies (e.g. Sturova 2001; Bennetts 2007), a large proportion of the scattered wave energy appears in a peak centred around the direction of the incident wave, which are generally wide and of moderate amplitude for the circular and crooked egg-shaped scatterers and tighter and of larger amplitude for the elliptical scatterers. The only instances in which a peak is not located in the direction of the incident wave is for the crooked egg-shaped

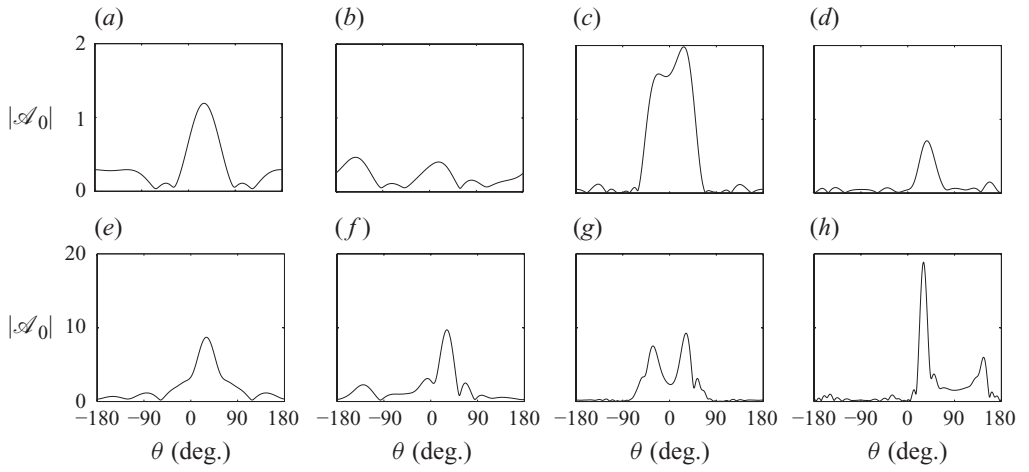

FIGURE 6. The modulus of the DFFA produced by floes, as a function of the azimuthal coordinate. The shape of the floe is: (*a*, *e*) circular, (*b*, *f*) crooked egg-shaped, (*c*, *g*) elliptical with *x*-stretch factor 3, and (*d*, *h*) elliptical with *y*-stretch factor 3. The radius of the circular floe is *a* and all of the floes share the same area. Results are shown for two wavelengths: (*a*–*d*) $\lambda = 2a$ and (*e*–*h*) $\lambda = a$.

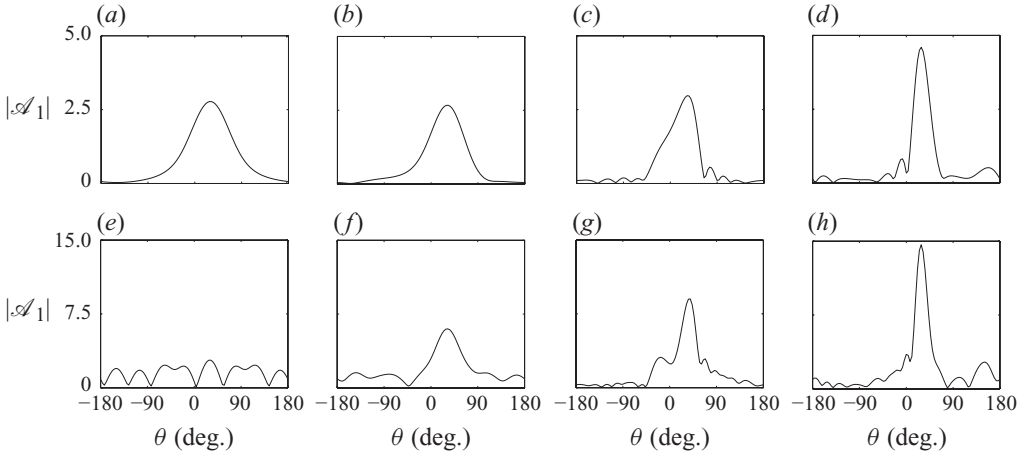

FIGURE 7. As in figure 6 but for polynyas.

floe forced by the longer incident wave (figure 6*b*) and the circular polynya forced by the shorter incident wave (figure 7*e*). This could indicate the presence of near resonance in these cases.

Whilst the far-field amplitudes of the circular and crooked egg-shaped scatterers are to some extent dominated by this primary scattering direction, both of the elliptical scatterers are distinguished with a secondary peak that is of approximately the same magnitude as the primary one. For the ellipse stretched in the *x* direction this secondary peak is roughly centred around $\theta = -30^\circ$ and in certain instances merges with the primary peak (most clearly demonstrated in figures 6*c* and 7*c*). In contrast, the ellipse stretched in the *y* direction has its secondary peak located around $\theta = 150^\circ$. This mimics the qualitative reflection properties predicted by the corresponding two-dimensional analyses, when the lengths of the ellipses are supposed

to extend infinitely in their stretched direction. As this is relative to the length scales involved in the problem, it is unsurprising that the similarity to the two-dimensional analogues becomes more evident for the shorter wavelengths. However, the peaks in these three-dimensional problems do occur over a significant range of angles and other smaller but non-trivial peaks exist in other directions.

The crooked egg-shaped scatterers also display evidence of a secondary peak around $\theta = -150^\circ$, although it is less prominent than those of the ellipses. With reference to the shape of the crooked egg, shown in figures 3 and 4, it can be seen that it is approximately symmetric with respect to the incident wave angle and this peak indicates direct reflection.

In general, there is more fine structure in the scattering response of the crooked egg-shaped floes and polynyas than their circular equivalents and even more so in the elliptical obstructions. This is reflected in a larger number of trial functions being required in the Galerkin expansions in these cases.

Meylan (2002) also investigated the effects of floe shape on its scattering response as a function of angle, albeit that produced only by the motion of the floe and averaged over its orientation. For the polygonal shapes considered in that work, in all cases scattering is dominated by the incident angle and consequently the differences between the floes were primarily in the magnitude of their response in this direction. Fine structure is also evident when the scattering caused by the floes is significant but decays in amplitude away from the incident angle.

Having ascertained that the directional properties of the radiated wave have a close relationship to the shape of the scattering source, it is now of interest to investigate how the overall strength of the radiated wave varies with shape. For this purpose, figures 8 and 9 show the SCCs, $\mathscr{S}_0$ or $\mathscr{S}_1$, as continuous functions of the non-dimensional wavenumber $a\kappa_0$, for the same four shapes of scatterer used in figures 6 and 7 and the incident wave angle $\tau = 30^\circ$. The range of wavenumbers considered in these figures approximately translates to free-surface wavelengths from 28 to 643 m and ice-coupled wavelengths from 79 to 628 m.

In all cases, there is a trend for the value of the SCC to rise with increasing wavenumber, until the wavelengths become relatively short and wave interactions within the scatterer results in fine structure in its response. These behaviours are to be expected and similar observations have been made in many other related studies. However, our interest is in how the characteristics of the SCCs differ between the various floe and polynya shapes.

It is reasonable to assert that for a large proportion of the range of wavenumbers considered here, the magnitude of the scattering responses between the different shapes are comparable. This is not the case though for the larger wavenumbers, towards the right-hand ends of the panels, where the shorter waves are able to differentiate between the shapes. Clearly, also the point at which the fine structure is instigated depends on the shape of the scatterer, which is implicitly understood to be related to its length with respect to the direction of the incident wave. Similarly, we see that the fine structure limit arises earlier for the polynyas, which is a consequence of identical values of κ_0 generating shorter waves within polynyas than in floes.

A prominent feature in the results displayed in figures 8 and 9 is the relatively wide troughs that occur for modest values of wavenumber and deviate from the otherwise locally monotonic increase in the SCC with wavenumber. The presence, position and dimensions of these minima appear to be very sensitive to the shape of the scattering source, and consequently, in their vicinity, the magnitude of scattering

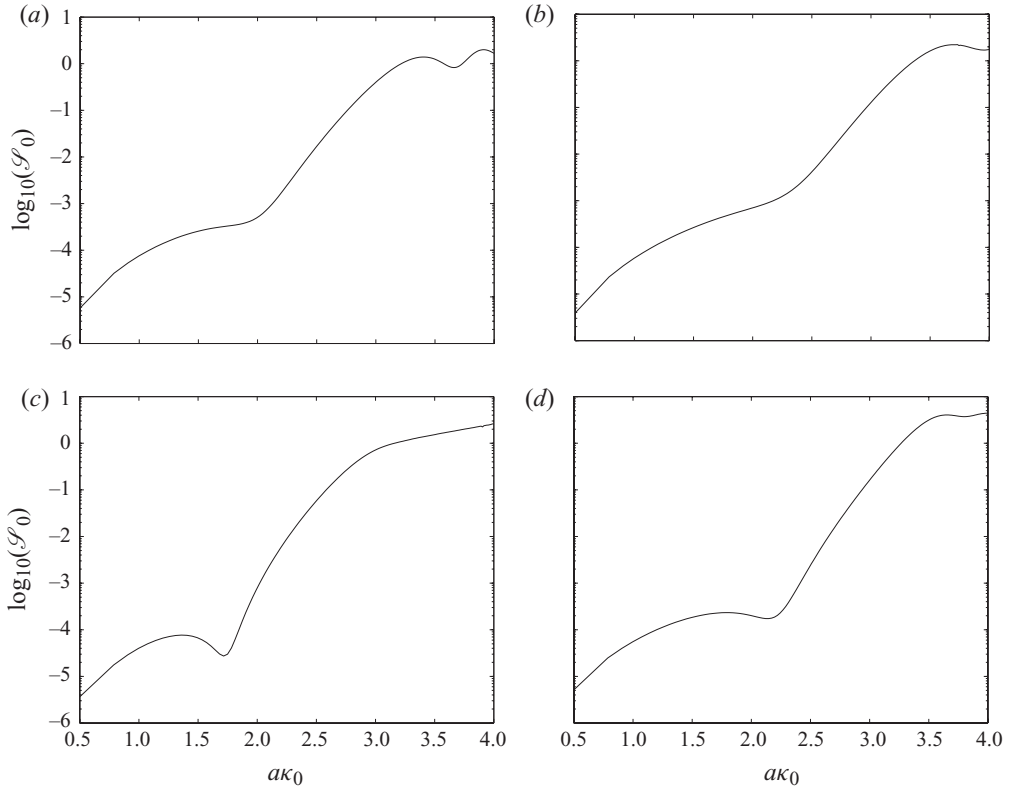

FIGURE 8. The SCC produced by floes, as a function of non-dimensional wavenumber. The shape of the floe is (*a*) circular, (*b*) crooked egg-shaped, (*c*) elliptical with *x*-stretch factor 3 and (*d*) elliptical with *y*-stretch factor 3. The radius of the circular floe is *a* and all of the floes share the same area.

produced by the different shapes can vary significantly (note that the ordinate axes are on a logarithmic scale in these figures). For instance, in the polynya problems the minima are pronounced when the polynya is circular or the *x*-stretched ellipse but are merely points of inflection for the other two shapes. However, for the floe problems the minima are most evident for the two ellipses. The inconsistency here demonstrates that the feature is not a product of a simple relationship between the length of the scatterer and the salient wavelength. It has also been found, in results not presented in this work, that the minimum is related to the flexural response of the ice.

Thus far the influence of the shape of the scatterer has only been considered in terms of the far-field response it produces. At this juncture attention is redirected towards the motions occurring within the scatterer itself and for each of the two different classes of geometry quantities that are of interest in the phenomena they model will be studied. This requires the solutions in the finite domains to be recovered from either of the integral expressions (3.7*b*) or (3.8*a*), depending on the problem in hand. Calculating values efficiently near to the boundary is a non-trivial task, as near-singular behaviour must be appropriately negotiated. However, a full account of the numerical techniques employed would be long and arduous and would detract from the current investigation.

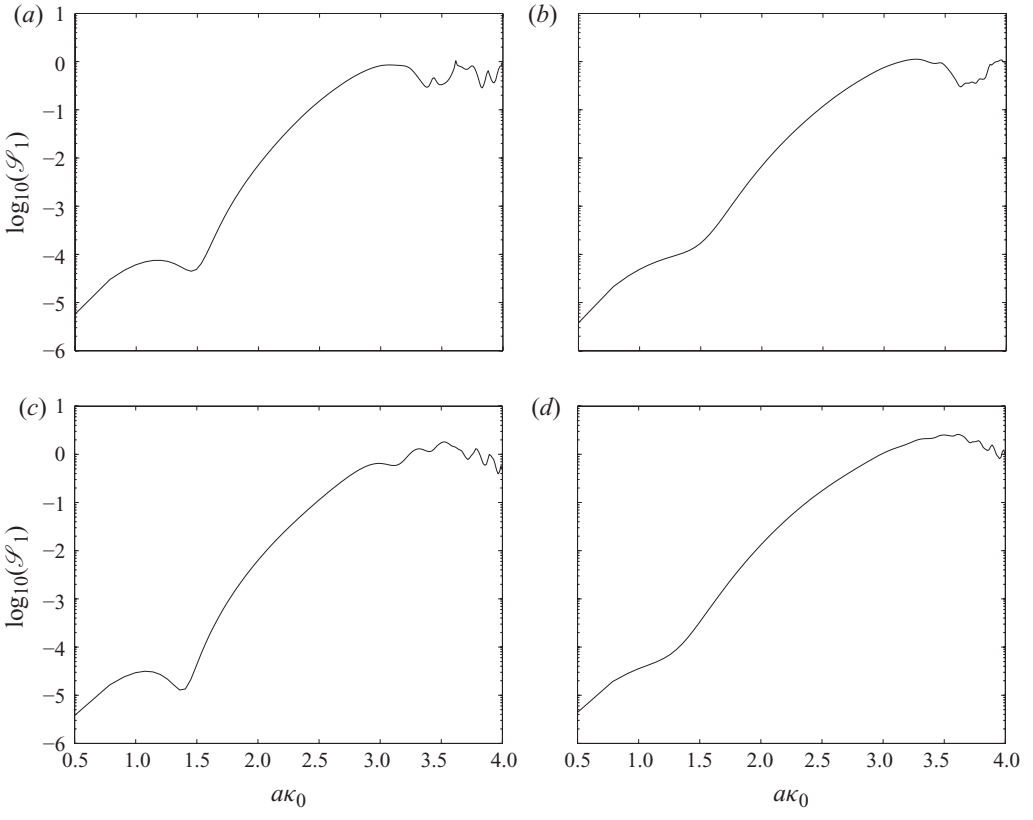

FIGURE 9. As in figure 8 but for polynyas.

We begin with the floe problem, for which curvature is relevant, as this may be used to deduce the strains it undergoes, which are directly related to its propensity to fracture (Squire *et al.* 1995). Therefore, a suitable quantity to study is the average curvature $\mathrm{Re}(\nabla^2 w) = \mathrm{Re}(\hat{w}/\beta)$ (see Timoshenko & Woinowsky-Krieger 1959), which is independent of direction and is easily recovered from our solution method.

Figure 10 displays the maximum of the average curvature at the instant $t = 0$ attained over the floe, denoted $\mathscr{M}_1 = \max\{\mathrm{Re}(\nabla^2 w) : \boldsymbol{x} \in \Omega_1\}$, for the same range of non-dimensional wavenumbers used to analyse the SCC. Results are given for the same four floe shapes used previously and for the incident wave angle $\tau = 30^\circ$, which is representative of results generated by all other angles.

Moving inwards from the left-hand end of each the individual panels, initially the qualitative behaviours of the maximum average curvatures are similar for the four floe shapes, with monotonic increase to a local maximum before a relatively sharp drop to approximately zero average curvature. The position of this maximum varies between $a\kappa_0 = 2.5$ and 3 for the different shapes and its height is also affected by the shape of the floe, with that of the crooked egg being notably smaller than the others. For all but the x-stretched ellipse, the curves then exhibit a second well-defined peak, which is larger in amplitude than the first, and the presence of a third can be inferred for larger wavenumbers not shown on these figures. Again the position and height of these second peaks are shape-dependent. In contrast, the x-stretched elliptical floe displays a series of three less well-defined peaks, which are smaller in magnitude than

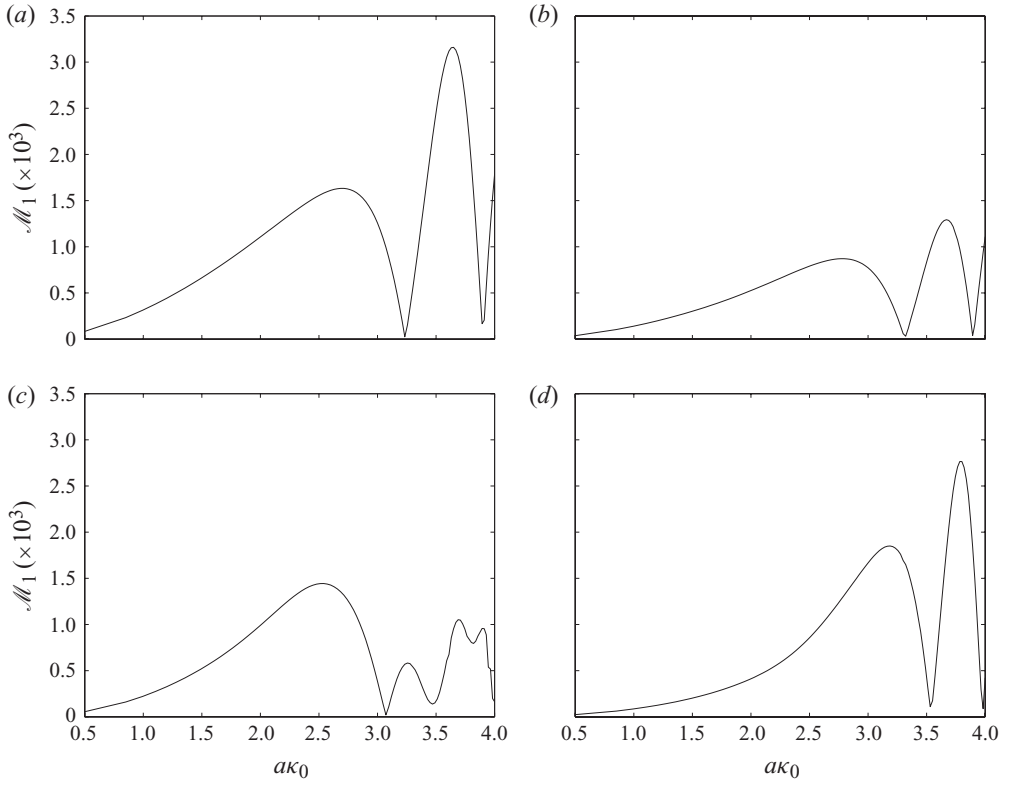

FIGURE 10. The maximum average curvature experienced by a floe, as a function of non-dimensional wavenumber. The shapes of the floes are as in figure 8.

the first. The more complicated structure of the average curvature seen here can be attributed to the extra length of the floe (in relation to the incident wave) allowing for more wave interactions within the floe.

In figure 11, results are presented for the maximum wave elevation at $t = 0$ in polynyas, denoted $\mathscr{M}_0 = \max\{\mathrm{Re}(\phi) \ : \ \boldsymbol{x} \in \Omega_0, z = 0\}$. The non-dimensional wavenumber used is ak_0, so that the wavelengths within the scatterer are consistent with figure 10. Again, for the smaller wavenumbers, here roughly $ak_0 < 1.5$, the shape of the obstruction does not greatly affect the motion it experiences, but this simply indicates that negligible scattering is occurring and the elevation is that of the passing incident wave.

For larger wavenumbers, where appreciable scattering occurs, the maximum wave elevation inside the polynyas is affected more strongly by their shape. Over the interval of wavenumbers considered, the elliptical polynyas display monotonic increase of $\mathscr{M}_0$, with the growth marginally more rapid for the x-stretched ellipse. The behaviours of the circular and crooked egg-shaped polynyas are more complicated. Both of these polynyas produce maximum elevations that grow relatively slowly at first but that suddenly increase and form local maxima. The sharp transition between these two states is due to a jump in the position within the polynyas at which the maximum elevation is attained. Although the qualitative nature of the results generated by these two shapes are alike, there are notable distinctions between them. In particular, the transition occurs for a larger wavenumber in the case of the crooked

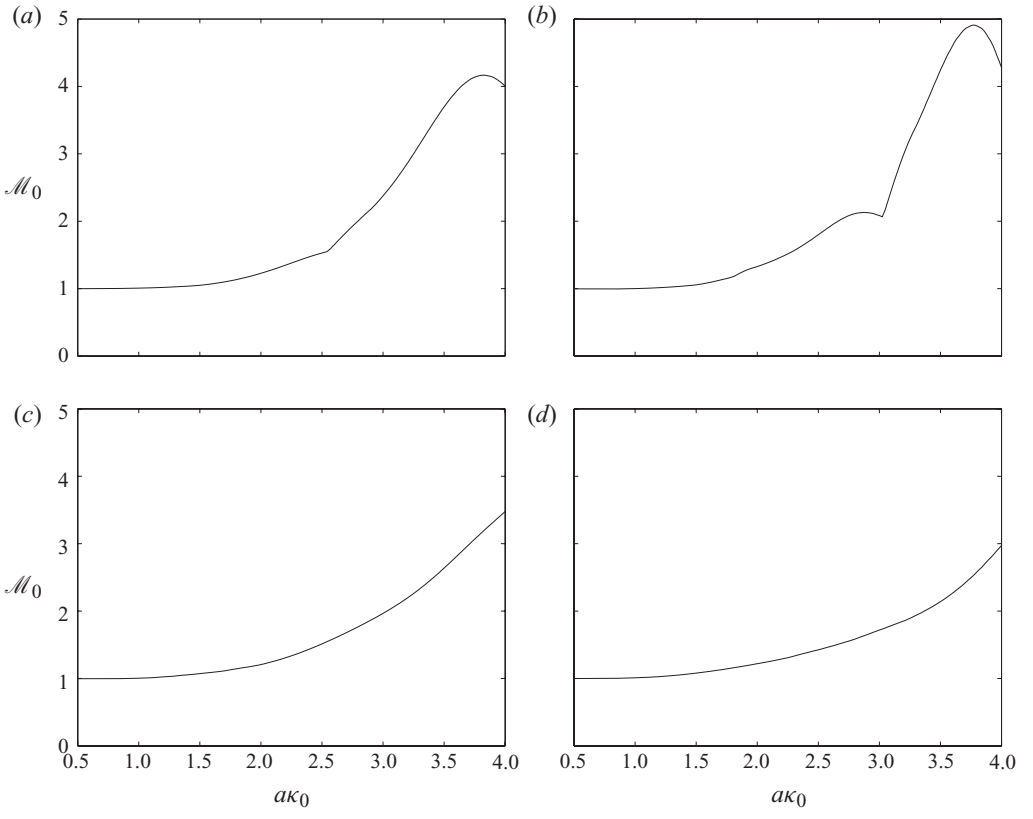

FIGURE 11. As in figure 10 but for the maximum surface displacement within polynyas.

egg-shaped polynya, and in the intervening interval a local maximum develops, and following the transition the gradient of its maximum elevation is far greater and results in a significantly larger maximum value of $\mathscr{M}_0$.

6. Summary and conclusions

A method for reducing problems of water-wave scattering by three-dimensional hydroelastic geometries to systems of one-dimensional integro-differential equations has been presented, where the scattering source is of an arbitrary shape. Two classes of geometry were considered, both involving a fluid domain of infinite extent that is partially covered by a floating thin-elastic plate. In one case, the covering is finite, representing an ice floe, and in the second the covering is infinite but containing a finite opening, representing an ice polynya.

Approximation methods, capable of delivering the full-linear solution to any desired tolerance, were employed. This consisted of an expansion of the velocity potential in a finite number of vertical modes in conjunction with a variational principle, followed by an implementation of Green's theorem in the plane using matrices of Green's functions. It was then shown how the resulting integro-differential equations could be solved efficiently through an application of the Galerkin technique. A Fourier basis underpinned this latter approximation, which is valid for all smooth boundaries. The extension to shapes involving piece-wise continuous boundaries is the topic of work that is currently in preparation.

The Archimedean draught of the floating plate was admitted in the model. It was recognised that this creates a geometry in which fluid must traverse a sharp corner and the expected singular behaviour of the fluid velocity that ensues at this point was embedded in the solution method using Gegenbauer polynomials in order to enhance convergence properties.

Numerical results initially illustrated the convergence properties of the method and then sought justification for modelling the shape of a floe or polynya. It was seen that the angular distribution of the most slowly decaying part of the diffracted wave field is highly sensitive to the shape of the scattering source. In particular, the dimensions of the floe or polynya accentuate reflection and transmission in certain directions. Furthermore, the otherwise monotonic increase in magnitude of the scattering response with increasing wavenumber displays a wide trough for modest wavelengths, and this feature varies significantly with the shape of scatterer.

Quantities of interest within the scatterers themselves were also studied. For the floe, this was the maximum average curvature and for the polynya the maximum wave elevation. In each case, it was seen that when non-trivial scattering occurs the shape of the scattering source is important both qualitatively and quantitatively, with certain features being created or accentuated or vice-versa.

The method outlined in this work will form the core of a model of ocean wave propagation through vast expanses of the ice-covered Arctic Ocean, which will be embedded in a global climate model as part of a project that is due to start this year. The numerical investigations that have been presented here are the first phase of the analysis that must be conducted during this forthcoming assignment. Prominent amongst the outstanding issues is to determine the importance of shape when a large field of interacting scatterers is considered.

It is hoped that the project will also furnish experimental data, which will provide a much needed means of validating mathematical models. Further such data are anticipated from a voyage to the Antarctic, which is scheduled for 2012 and will dedicate time to recording wave evolution in ice infested waters. Moreover, these field data will be complemented by wave tank experiments that are to be performed by collaborators at the Laboratoire de Mécanique des Fluides, Ecole Centrale de Nantes later this year, in which the interaction of water waves with a small number of synthetic floes will be studied under controlled conditions.

The authors would like to thank Vernon Squire (University of Otago) for his advice on the geophysical aspects relating to this work. L.G.B. is supported by the Marsden Fund Council from Government funding administered by the Royal Society of New Zealand and by the University of Otago. T.D.W. holds a post-doctoral fellowship from the New Zealand Foundation of Research, Science and Technology.

Appendix. Circular obstructions

The solution method outlined in § 3 has been developed for floes and polynyas of arbitrary shape and the system of equations that has been generated can hence appear somewhat abstract. With this in mind, it is pertinent to consider a simplified obstruction, specifically a circular floe or polynya, to illustrate an application of the method in an analytic setting. This has the added benefit that alternative solution methods exist (e.g. Meylan & Squire 1996; Peter *et al.* 2004), which enables us to verify our results.

For a circular obstruction that, without loss of generality, we may suppose to be of unit radius, the contour Υ is defined using the polar coordinates, so that the Galerkin expansions (3.17*a*, *b*) are Fourier series with respect to the azimuthal coordinate. These Fourier series may be mirrored in the other functions involved in the problems by making use of Graf's addition formulae (cf. Abramowitz & Stegun 1964, §9). Firstly, for the incident wave field via

$$\mathrm{e}^{\mathrm{i}k(x\cos\tau+y\sin\tau)}=\sum_{m\in\mathbb{Z}}J_m(kr)I_m, \tag{A 1}$$

where the scalars I_m depend on the incident angle τ and are easily calculated. We thus denote the incident waves as

$$\boldsymbol{\Phi}^{(I)}(\boldsymbol{x})=\frac{1}{2\pi}\sum_{m\in\mathbb{Z}}\boldsymbol{J}_{0,m}(r)\boldsymbol{i}_{0,m}\mathrm{e}^{\mathrm{i}m\theta},\quad \widetilde{\boldsymbol{\Psi}}^{(I)}(\boldsymbol{x})=\frac{1}{2\pi}\sum_{m\in\mathbb{Z}}\boldsymbol{J}_{1,m}(r)\boldsymbol{i}_{1,m}\mathrm{e}^{\mathrm{i}m\theta}, \tag{A 2}$$

where the vectors $\boldsymbol{i}_{i,m}$ $(i=0,1)$ are of length $N+1$ and $N+3$, respectively, and are known, and the matrices $\boldsymbol{J}_{i,m}$ contain Bessel functions and will be defined shortly. For the matrices of Green's functions explicit expansions occur as a Fourier series with respect to the angle between the source and field points, using

$$H_0(kR)=\sum_{m\in\mathbb{Z}}J_m(kr_-)H_m(kr_+)\mathrm{e}^{\mathrm{i}m(\theta-\vartheta)},\quad r_\pm=\max/\min\{r,\varrho\}, \tag{A 3}$$

where H_m is the Hankel function of the first kind, order m.

In order to use the above expansion of the Hankel function in the method outlined in §3, we must recall that there is a logarithmic singularity at the point $R=0$ that manifests as non-convergence of the series (A 3) at this point. The series representation therefore cannot be differentiated directly, and instead its normal derivative is found to be

$$\begin{aligned}\partial_r H_0(kR)&=\sum_{m\in\mathbb{Z}}\left\{J_m'(k)H_m(k)+\frac{\mathrm{i}}{\pi}\right\}\mathrm{e}^{\mathrm{i}m(\theta-\vartheta)}\\&=\sum_{m\in\mathbb{Z}}\left\{J_m(k)H_m'(k)-\frac{\mathrm{i}}{\pi}\right\}\mathrm{e}^{\mathrm{i}m(\theta-\vartheta)},\end{aligned} \tag{A 4}$$

when $|\boldsymbol{x}|,|\boldsymbol{X}|=1$, and in which a prime indicates differentiation with respect to r.

Unsurprisingly, due to the circular geometry, the Fourier modes decouple, so that when solving the equations produced by the Galerkin technique there is no need to amalgamate the unknowns, as in (3.19*a*, *b*) or (3.20*a*, *b*). As explicit Fourier expansions of the matrices of Green's functions and incident wave are available, it is possible to calculate all of the inner products needed to calculate the unknowns on Υ analytically. After some manipulation, the system of equations given by implementing the Galerkin technique on the integro-differential equations may be written as

$$\boldsymbol{H}_{0,m}'\boldsymbol{p}_{0,m}-\boldsymbol{H}_{0,m}\boldsymbol{A}_0^{-1}\boldsymbol{V}_0\boldsymbol{u}_m=\frac{2\mathrm{i}}{\pi}\boldsymbol{i}_{0,m},\quad \boldsymbol{E}_{J,m}\boldsymbol{q}_{1,m}-\boldsymbol{G}_{J,m}\boldsymbol{A}_1^{-1}\boldsymbol{V}_1\boldsymbol{u}_m=\boldsymbol{0}, \tag{A 5a}$$

on $r=1$, for the floe problem, and

$$\boldsymbol{J}_{0,m}'\boldsymbol{p}_{0,m}-\boldsymbol{J}_{0,m}\boldsymbol{A}_0^{-1}\boldsymbol{V}_0\boldsymbol{u}_m=\boldsymbol{0},\quad \boldsymbol{E}_{H,m}\boldsymbol{q}_{1,m}-\boldsymbol{G}_{H,m}\boldsymbol{A}_1^{-1}\boldsymbol{V}_1\boldsymbol{u}_m=\frac{2\mathrm{i}}{\pi}\boldsymbol{i}_{1,m}, \tag{A 5b}$$

on $r=1$, for the polynya problem ($m=-M,\ldots,M$). The size $(N+1)$-square matrices $\boldsymbol{J}_{0,m}$ and $\boldsymbol{H}_{0,m}$ in these equations are

$$\boldsymbol{J}_{0,m}(r)=\lceil J_m(k_0r),\ldots,J_m(k_Nr)\rfloor,\quad \boldsymbol{H}_{0,m}(r)=\lceil H_m(k_0r),\ldots,H_m(k_Nr)\rfloor \tag{A 6}$$

and the size $(N+3)$-square matrices $\boldsymbol{E}_{X,m}$ and size $(N+3)\times(N+1)$ matrices $\boldsymbol{G}_{X,m}$ $(X=J,H)$ are

$$\{\boldsymbol{E}_{X,m}\}_{j,i}=\{\boldsymbol{X}'_{1,m}\}_{j,i},\quad \{\boldsymbol{G}_{X,m}\}_{j,i}=\{\boldsymbol{X}_{1,m}\}_{j,i}\quad (j=1,\ldots,N+3,\ i=1,\ldots,N+1), \tag{A 7}$$

$$\{\boldsymbol{E}_{X,m}\}_{j,N+2}=\{\boldsymbol{X}'_{1,m}\}_{j,N+2}-\tilde{\beta}m^2\{\boldsymbol{X}'_{1,m}-\boldsymbol{X}_{1,m}\}_{j,N+3}, \tag{A 8}$$

$$\{\boldsymbol{E}_{X,m}\}_{j,N+3}=-\{\boldsymbol{X}_{1,m}\}_{j,N+2}+\tilde{\beta}\{\boldsymbol{X}'_{1,m}-m^2\boldsymbol{X}_{1,m}\}_{j,N+3}, \tag{A 9}$$

for $j=1,\ldots,N+3$ and $X=J$ or H, in which the matrices

$$\boldsymbol{J}_{1,m}(r)=\boldsymbol{C}\lceil J_m(\kappa_0r),\ldots,J_m(\kappa_Nr),J_m(\kappa_{-1}r),J_m(\kappa_{-2}r)\rfloor\boldsymbol{C}^{-1} \tag{A 10}$$

and

$$\boldsymbol{H}_{1,m}(r)=\boldsymbol{C}\lceil H_m(\kappa_0r),\ldots,H_m(\kappa_Nr),H_m(\kappa_{-1}r),H_m(\kappa_{-2}r)\rfloor\boldsymbol{C}^{-1} \tag{A 11}$$

are both size $(N+3)$-square. Equations (A 5*a*) or (A 5*b*) are combined with the joining condition (2.24*a*), which also decouples to give

$$\boldsymbol{V}_0^{\mathrm{T}}\boldsymbol{p}_{0,m}=\boldsymbol{V}_1^{\mathrm{T}}\boldsymbol{p}_{1,m}\quad (m=-M,\ldots,M), \tag{A 12}$$

in order to retrieve $\boldsymbol{p}_{0,m}$, $\boldsymbol{q}_{1,m}$ ($\boldsymbol{p}_{1,m}$) and $\boldsymbol{u}_m$ for each $m=-M,\ldots,M$ independently.

It is then possible to obtain the solution throughout the horizontal plane in terms of the values calculated on Υ. Using our expressions for the incident wave and matrices of Green's functions in the relevant integral expression (3.7*a*, *b*) or (3.8*a*, *b*), we find that

$$\boldsymbol{\Phi}(\boldsymbol{x})=\boldsymbol{\Phi}^{(I)}(\boldsymbol{x})+\frac{1}{2\pi}\sum_{m=-M}^{M}\boldsymbol{H}_{0,m}(r)\boldsymbol{a}_{0,m}\mathrm{e}^{\mathrm{i}m\theta},\ \widetilde{\boldsymbol{\Psi}}(\boldsymbol{x})=\frac{1}{2\pi}\sum_{m=-M}^{M}\boldsymbol{J}_{1,m}(r)\boldsymbol{a}_{1,m}\mathrm{e}^{\mathrm{i}m\theta}, \tag{A 13a}$$

where $r>1$ and $r<1$, respectively, for the floe problem, and

$$\widetilde{\boldsymbol{\Psi}}(\boldsymbol{x})=\widetilde{\boldsymbol{\Psi}}^{(I)}(\boldsymbol{x})+\frac{1}{2\pi}\sum_{m=-M}^{M}\boldsymbol{H}_{1,m}(r)\boldsymbol{b}_{1,m}\mathrm{e}^{\mathrm{i}m\theta},\ \boldsymbol{\Phi}(\boldsymbol{x})=\frac{1}{2\pi}\sum_{m=-M}^{M}\boldsymbol{J}_{0,m}(r)\boldsymbol{b}_{0,m}\mathrm{e}^{\mathrm{i}m\theta}, \tag{A 13b}$$

likewise, for the polynya problem, where the vectors $\boldsymbol{a}_{i,m}$ and $\boldsymbol{b}_{i,m}$ are

$$\boldsymbol{a}_{0,m}=\frac{\pi}{2\mathrm{i}}\left(\boldsymbol{J}_{0,m}\boldsymbol{A}_0^{-1}\boldsymbol{V}_0\boldsymbol{u}_m-\boldsymbol{J}'_{0,m}\boldsymbol{p}_{0,m}\right),\ \boldsymbol{a}_{1,m}=\frac{\pi}{2\mathrm{i}}\left(\boldsymbol{E}_{H,m}\boldsymbol{p}_{0,m}-\boldsymbol{G}_{H,m}\boldsymbol{A}_1^{-1}\boldsymbol{V}_1\boldsymbol{u}_m\right) \tag{A 14a}$$

and

$$\boldsymbol{b}_{0,m}=\frac{\pi}{2\mathrm{i}}\left(\boldsymbol{H}'_{0,m}\boldsymbol{p}_{0,m}-\boldsymbol{H}_{0,m}\boldsymbol{A}_0^{-1}\boldsymbol{V}_0\boldsymbol{u}_m\right),\ \boldsymbol{b}_{1,m}=\frac{\pi}{2\mathrm{i}}\left(\boldsymbol{G}_{J,m}\boldsymbol{A}_1^{-1}\boldsymbol{V}_1\boldsymbol{u}_m-\boldsymbol{E}_{J,m}\boldsymbol{p}_{0,m}\right), \tag{A 14b}$$

in which the matrices $\boldsymbol{J}_{0,m}$, $\boldsymbol{H}_{0,m}$, $\boldsymbol{E}_{X,m}$ and $\boldsymbol{G}_{X,m}$ $(X=J,H)$ are evaluated on $r=1$.

Let us now consider another solution method that is restricted to circular obstructions. In this case, a logical starting point would be to expand all of the unknowns as truncated Fourier series throughout the horizontal plane. Seeking separation solutions and imposing boundedness at the origin and the far-field conditions leads to expressions identical to (A 13*a*, *b*) but in which the vectors $\boldsymbol{a}_{i,m}$ and $\boldsymbol{b}_{i,m}$ $(i=0,1)$ are unknown. To obtain these quantities, the solutions in the ice-covered

and free-surface fluid domains must be matched at their common boundary Υ. For consistency of notation with the previous solution method, let

$$\boldsymbol{p}_{0,m} = \boldsymbol{p}_{0,m}(r) \equiv \boldsymbol{J}_{0,m}(r)\boldsymbol{i}_{0,m} + \boldsymbol{H}_{0,m}(r)\boldsymbol{a}_{0,m} \quad \text{and} \quad \tilde{\boldsymbol{q}}_{1,m} = \tilde{\boldsymbol{q}}_{1,m}(r) \equiv \boldsymbol{J}_{1,m}(r)\boldsymbol{a}_{1,m}, \quad \text{(A 15)}$$

for the floe problem, and

$$\boldsymbol{p}_{0,m}(r) \equiv \boldsymbol{J}_{0,m}(r)\boldsymbol{b}_{0,m} \quad \text{and} \quad \tilde{\boldsymbol{q}}_{1,m}(r) \equiv \boldsymbol{J}_{1,m}(r)\boldsymbol{i}_{1,m} + \boldsymbol{H}_{1,m}(r)\boldsymbol{b}_{1,m}, \quad \text{(A 16)}$$

for the polynya problem. It is then simple to show that the following identities hold:

$$\boldsymbol{H}'_{0,m}\boldsymbol{p}_{0,m} - \boldsymbol{H}_{0,m}\boldsymbol{p}'_{0,m} = \frac{2\mathrm{i}}{\pi}\boldsymbol{i}_{0,m}, \quad \boldsymbol{J}'_{1,m}\tilde{\boldsymbol{q}}_{1,m} - \boldsymbol{J}_p\tilde{\boldsymbol{q}}'_{1,m} = \boldsymbol{0}, \quad \text{(A 17}a\text{)}$$

for the former problem, and

$$\boldsymbol{J}_{0,m}\boldsymbol{p}_{0,m} - \boldsymbol{J}_{0,m}\boldsymbol{p}'_{0,m} = \boldsymbol{0}, \quad \boldsymbol{H}'_{1,m}\tilde{\boldsymbol{q}}_{1,m} - \boldsymbol{H}_{1,m}\tilde{\boldsymbol{q}}'_{1,m} = \frac{2\mathrm{i}}{\pi}\boldsymbol{i}_{1,m}, \quad \text{(A 17}b\text{)}$$

for the latter problem. In addition to the decoupling of the joining condition that approximates continuity of fluid pressure, the conditions that represents continuity of fluid velocity do likewise, so that

$$\boldsymbol{V}_0^{\mathrm{T}}\boldsymbol{p}_{0,m} = \boldsymbol{V}_1^{\mathrm{T}}\boldsymbol{p}_{1,m}, \quad \boldsymbol{A}_0\boldsymbol{p}_{0,m} = \boldsymbol{V}_0\boldsymbol{u}_m, \quad \boldsymbol{A}_1\boldsymbol{p}_{1,m} = \boldsymbol{V}_1\boldsymbol{u}_m \quad (m = -M, \ldots, M), \quad \text{(A 18}a\text{)}$$

at $r = 1$, where the vector $\boldsymbol{p}_{1,m}$ denotes the first $N+1$ entries of $\tilde{\boldsymbol{q}}_{1,m}$. The free-edge conditions (2.17*a*, *b*) also decouple, resulting in

$$\hat{w}_m - \tilde{\beta}(w'_m - m^2 w_m) = 0, \quad \hat{w}'_m - m^2\tilde{\beta}(w'_m - w_m) = 0 \quad (m = -M, \ldots, M), \quad \text{(A 18}b\text{)}$$

where w_m and $\hat{w}_m$ are the $(N+2)$th and $(N+3)$th entries of $\tilde{\boldsymbol{q}}_{1,m}$, respectively. This solution is identical to that given by Bennetts (2007, § 9), although this previous work was restricted to equal truncations in the vertical plane $N = U$ and used ice-covered fluid vertical modes in place of Gegenbauer polynomials.

Taking the relevant components of identities (A 17*a*, *b*) at the boundary $r = 1$ along with the conditions (A 18*a*, *b*) is visibly equivalent to the corresponding components of the system (A 5*a*, *b*) combined with the joining condition (A 12) that is used to find the unknowns in the previous solution method. The form of the vector amplitudes (A 14*a*, *b*) can also be found for this new method using identities (A 17*a*, *b*). It is therefore clear that the solution method that we have constructed in this work, which may be applied to arbitrary boundaries, reduces to the method of simple matching when the obstruction is circular.

REFERENCES

Abramowitz, M. & Stegun, I. 1964 *Handbook of Mathematical Functions*. Dover.

Bennetts, L. G. 2007 Wave scattering by ice sheets of varying thickness. PhD thesis, University of Reading, Berkshire, UK.

Bennetts, L. G., Biggs, N. R. T. & Porter, D. 2007 A multi-mode approximation to wave scattering by ice sheets of varying thickness. *J. Fluid Mech.* **579**, 413–443.

Bennetts, L. G., Biggs, N. R. T. & Porter, D. 2009 Wave scattering by an axisymmetric ice floe of varying thickness. *IMA J. Appl. Math.* **74**, 273–295.

Bennetts, L. G., Peter, M. A., Squire, V. A. & Meylan, M. H. 2010 A three-dimensional model of wave attenuation in the marginal ice zone. *J. Geophys. Res.*, doi:10.1029/2009JC005982.

Bennetts, L. G. & Squire, V. A. 2009 Wave scattering by multiple rows of circular ice floes. *J. Fluid Mech.* **639**, 213–238.

Chung, H. & Linton, C. M. 2005 Reflection and transmission of waves across a gap between two semi-infinite elastic plates on water. *Q. J. Mech. Appl. Maths* **58**, 1–15.

Evans, D. V. & Peter, M. A. 2009 Asymptotic reflection of linear water waves by submerged horizontal porous plates. *J. Engng Maths*, doi:10.1007/s10665-009-9355-2.

Evans, D. V. & Porter, R. 2003 Wave scattering by narrow cracks in ice sheets floating on water of finite depth. *J. Fluid Mech.* **484**, 143–165.

Fox, C. & Squire, V. A. 1994. On the oblique reflexion and transmission of ocean waves at shore fast sea ice. *Phil. Trans. R. Soc. Lond.* A **347**, 185–218.

Kohout, A. L. & Meylan, M. H. 2008 An elastic plate model for wave attenuation and ice floe breaking in the marginal ice zone. *J. Geophys. Res.* **113** (C09016), doi:10.1029/2007JC004434.

Langhorne, P. J., Squire, V. A. & Haskell, T. G. 2001 Lifetime estimation for a fast ice sheet subjected to ocean swell. *Ann. Glaciol.* **33**, 333–338.

Linton, C. & Chung, H. 2003 Reflection and transmission at the ocean/sea-ice boundary. *Wave Motion* **38**, 43–52.

Manam, S. R., Bhattarchajee, J. & Sahoo, T. 2006 Expansion formulae in wave structure interaction problems. *Proc. R. Soc. Lond.* A **462**, 263–287.

Meylan, M. H. 2002 Wave response of an ice floe of arbitrary geometry. *J. Geophys. Res.* **107** (C1), doi:10.1029/2000JC000713.

Meylan, M. H. & Squire, V. A. 1996 Response of a circular ice floe to ocean waves. *J. Geophys. Res.* **101**, 8869–8884.

Norris, A. N. & Vemula, C. 1995 Scattering of flexural waves on thin plates. *J. Sound Vib.* **181** (1), 115–125.

Ohkusu, M. & Namba, Y. 2004 Hydroelastic analysis of a large floating structure. *J. Fluids Struct.* **19**, 543–555.

Peter, M. A. & Meylan, M. H. 2009 Water-wave scattering by vast field of bodies. *SIAM J. Appl. Maths* **70** (5), 1567–1586.

Peter, M. A., Meylan, M. H. & Chung, H. 2004 Wave scattering by a circular elastic plate in water of finite depth: a closed form solution. *Intl J. Offshore Polar Engng* **14** (2), 81–85.

Porter, R. & Evans, D. V. 2007 Diffraction of flexural waves by finite straight cracks in an elastic sheet over water. *J. Fluids Struct.* **23** (2), 309–327.

Porter, R. & Porter, D. 2000 Water wave scattering by a step of arbitrary profile. *J. Fluid Mech.* **411**, 131–164.

Porter, D. & Porter, R. 2004 Approximations to wave scattering by an ice sheet of variable thickness over undulating bed topography. *J. Fluid Mech.* **509**, 145–179.

Porter, D. & Staziker, D. J. 1995 Extensions of the mild-slope equation. *J. Fluid Mech.* **509**, 145–179.

Squire, V. A. 2007 Of ocean waves and sea-ice revisited. *Cold Reg. Sci. Technol.* **49**, 110–133.

Squire, V. A. 2008 Synergies between VLFS hydroelasticity and sea ice research. *Intl J. Offshore Polar Engng* **18**, 1–13.

Squire, V. A. & Dixon, T. W. 2000 An analytic model for wave propagation across a crack in an ice sheet. *Intl J. Offshore Polar Engng* **10** (3), 173–176.

Squire, V. A., Dugan, J. P., Wadhams, P., Rottier, P. J. & Liu, A. K. 1995 Of ocean waves and sea ice. *Annu. Rev. Fluid Mech.* **27**, 115–168.

Squire, V. A., Vaughan, G. L. & Bennetts, L. G. 2009 Ocean surface wave evolvement in the Arctic Basin. *Geophys. Res. Lett.* **36** (L22502).

Sturova, I. V. 2001 The diffraction of surface waves by an elastic platform floating on shallow water. *J. Appl. Math. Mech.* **65**, 109–117.

Timoshenko, S. & Woinowsky-Krieger, S. 1959 *Theory of Plates and Shells*, 2nd edn. McGraw-Hill.

Vaughan, G. L., Bennetts, L. G. & Squire, V. A. 2009 The decay of flexural-gravity waves in long sea-ice transects. *Proc. R. Soc. Lond.* A **465**, 2785–2812.

de Veubeke, B. F. 1979 *Cours Delasticite*. Springer.

Wang, C. D. & Meylan, M. H. 2004 A higher-order-coupled boundary element and finite element method for the wave forcing of a floating elastic plate. *J. Fluids Struct.* **19**, 557–572.

Watanabe, E., Utsunomiya, T. & Wang, C. 2004 Hydroelastic analysis of pontoon-type VLFS: a literature survey. *Engng Struct.* **26** (2), 245–256.

Williams, T. D. 2006 Reflections on ice: scattering of flexural-gravity waves by irregularities in Arctic and Antarctic ice sheets. PhD thesis, Otago University, Dunedin, New Zealand.

Williams, T. D. & Porter, R. 2009 The effect of submergence on the scattering by the interface between two floating plates. *J. Fluids. Struct.* **25** (5), 777–793.

Williams, T. D. & Squire, V. A. 2004 Oblique scattering of plane flexural-gravity waves by heterogeneities in sea-ice. *Proc. R. Soc. Lond.* A **460**, 3469–3497.

Williams, T. D. & Squire, V. A. 2010 On the estimation of sea-ice thickness using wave observations. *Dyn. Atmos. Oceans* **49** (2–3), 215–233.